

Economic analysis of heat pump integrated icecream making plant

Kalpan Patel

Design Engineer, Synergy Agro Tech Private Limited, Ahmedabad, Gujarat, India

Dilip Sarda

Managing Director, Synergy Agro Tech Private Limited, Ahmedabad, Gujarat, India

Balkrushna Shah

Assistant Professor, Mechanical Dept, Institute of Technology, Nirma University, Ahmedabad, Gujarat, India

ABSTRACT: Worldwide icecream is considered favourite dessert and consumption is increasing day by day. Icecream manufacturing consists of process like pasteurization, homogenization, chilling of mix and freezing. Around 65°-70°C temperature is required for pasteurization which is achieved by using hot water generated by electricity or gas or other fuels. Around 1°C chilled water is required to be supplied by refrigeration for cooling of the icecream mix. Aging of this mix is to be done for 5-6 hr in aging tank at 4°C and then it is taken in the freezer to produce icecream. Also, icecream plant requires large amount of hot water for cleaning and sanitizing of the equipments, piping, utensils and washing of floors. As in icecream manufacturing process both heating and cooling are required, use of heat-pump may prove to be a better solution. In this paper detailed economic analysis has been given for heat pump integrated ice cream making plant. The aim of process integration is to reduce the energy consumption and thereby an operating cost of the icecream making. Heating and cooling requirement for 2000 liter of icecream production per day have been calculated. Suitable heat pump has been integrated in the existing plant in order to have benefit of heating utility for partial pasteurization upto temperature 58°C and cooling utility for the partial cooling of mix upto temperature 18°C. Saving of around 34% of energy consumption is resulted in heat pump integrated systems. As per the calculations simple payback period for modified icecream making plant with heat pump is 2.2 years.

1. INTRODUCTION

Study of energy saving in an industrial process using heat pump integration begins with collection of data, finding out scope of integration in existing system and finally modifying the system. Heat pump is widely used in domestic application like space heating in cold countries. Use of heat pump in industry is very advantageous if both heating and cooling utility are required in the process. A.H. Zaidi et al. (1979) in their study explained use of heat pump in dairy industry. They integrated heat pump system with Pasteurizers, Evaporators, Spray dryers, Refrigeration and Cold storage equipment which are used in dairy plant.

Icecream making is one such process where simultaneously heating and cooling are required. After studying flow diagram of existing process it is found that there are certain areas where integration of heat pump is possible to some extent for pasteurization, cooling, aging and in freezer. Also icecream industry requires lot of hot water for cleaning and sanitizing utensils and washing of shop floor. This requirement can also be fulfilled by heat pump. J. Ubbels and S. Bouman (1979) studied the opportunities of saving of energy in milk cooling and heating water on farms. They showed integration of heat pump in refrigerated farm tank with the use of precooler and explained saving of energy analytically and experimentally where water is being heated with Heat pump. Pasteurization is a process which is used in dairy and icecream industry requires heat energy. Thermal and economic analysis of heat pump and auxiliary heater for the use of milk pasteurization process is carried out on heat transfer basis and life cycle cost of system is evaluated. Omer omakli et al. [Soylemez M.S.] studied water source heat pump integrated in the existing system and experiments were carried out for variation in COP with time at certain temperatures. In this paper an icecream mix plant of 500 liter/hr capacity is taken as a case study and energy saving by integrating heat pump is calculated. A new process flow diagram is also generated. Economic analysis of the project is carried out to ensure its viability considering 2000L/day icecream production.

Nomenclature

m	Mass flow rate, (kg/s)	Q	Load, (kW)
ΔT	Temperature difference, (°C)	PHE	Plate heat exchanger
Cp	Specific heat, (kJ/kg.K)	COP	Coefficient of performance

2 PROCESS INTEGRATION METHODOLOGY

1.1 Introduction to case study

The industrial process that is used for this analysis is an icecream mix manufacturing unit 500 liter/hr capacity and total production 2000L/day of icecream. Here it may be noted that 1 liter icecream mix can produce 2 liter of icecream considering overrun of 100%.

1.2 Process operation and parameters

The process operation steps in a conventional ice-cream making plant are summarized in Fig 1.

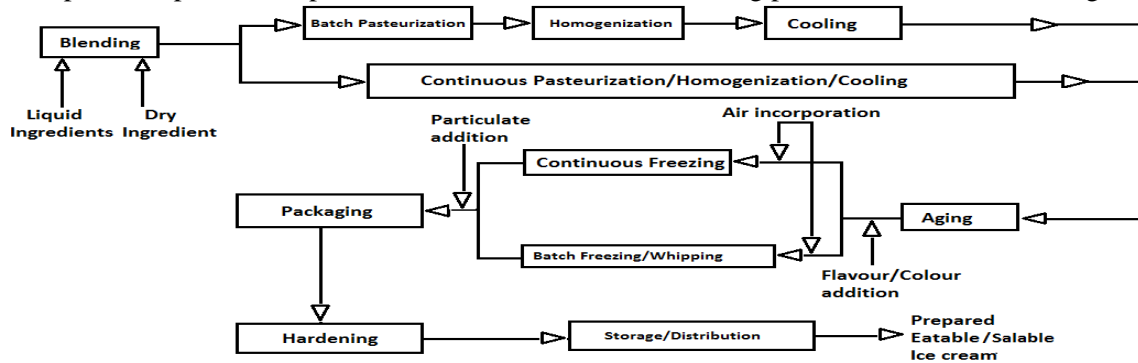


Figure 1. Process description

For the case study existing ice-cram making plant with following details have been considered.

Table 1. Details of existing icecream making plant

Process	Equipment	Capacity (L/hr)	Operating temperature (°C)
Pasteurization	Pasteurizer, Electric heater	500	20° to 70°
Homogenization	Homogenizer	500	70°
Cooling	P.H.E	500	70° to 8°
Aging	Aging tank	1000	8° to 4°
Storage	Aging tank	1000	4°
Icecream production	Continues freezer	400	4° to -5°
Cleaning	Pasteurizer	500	30° to 60°

As the capacity of Pasteurizer, Homogenizer and P.H.E is 500 liter, 2 batches of icecream mix is required for the production of 2000 liter icecream per day.

1.3 Process flow diagrams:

The actual process diagram of existing plant is shown in Fig 2(a). Heat pump is used to generate hot water of 60°C and cold water of 10°C. Hot and cold water are stored in its respective insulated tanks. Hot water is used for partial heating of icecream mix upto 58°C for pasteurization process. Thus the use of electric heater is reduced for pasteurization process. Cold water is used for second stage cooling in P.H.E to cool icecream mix upto 18°C. The modified process flow diagram with heat pump is shown in Fig 2(b). The hot water required for cleaning purpose is drawn directly from hot water storage tanks.

1.4 Analytical calculation of energy usage

Heating and cooling requirement for each process is worked out using following equation.

$$Q = m \times C_p \times \Delta T \quad (1)$$

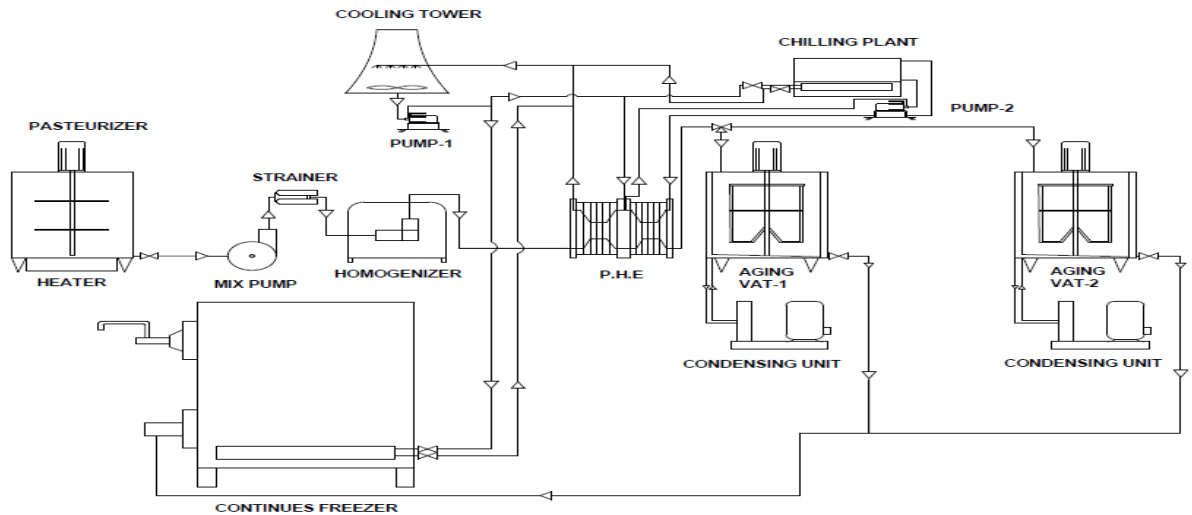


Figure 2(a). Existing icecream making plant

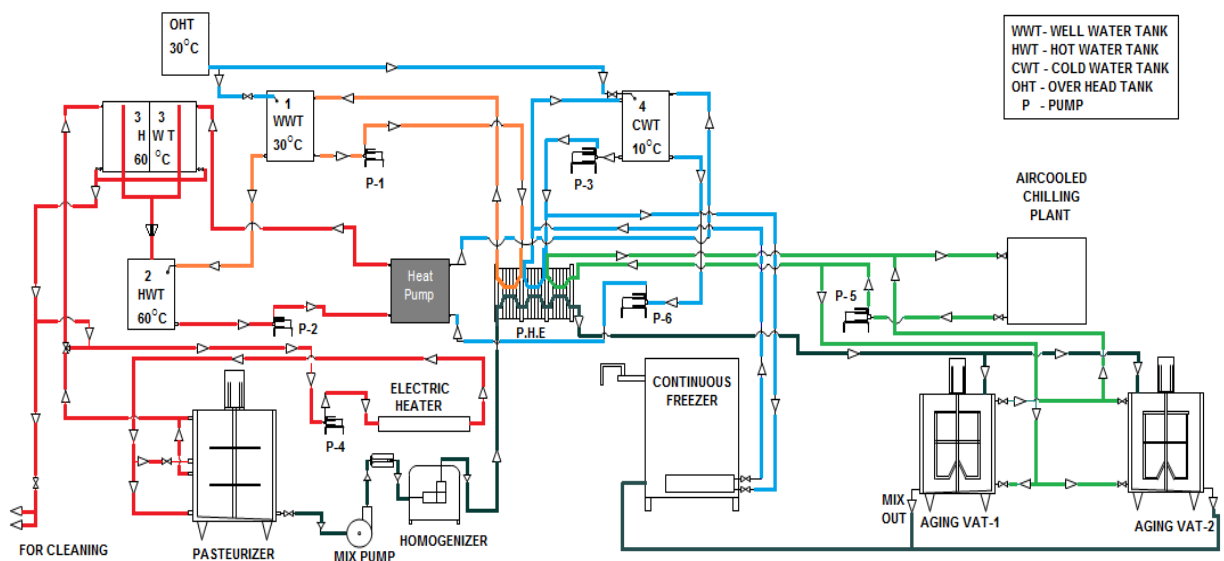


Figure 2(b). Heat pump integrated icecream making plant

The electricity required for heating is worked out using the formula (1). While electricity required for other equipments is worked out considering rated motor capacity with 0.8 as load factor. C.O.P of the whole system cannot be worked out but Danfoss compressor selection charts [Danfoss commercial compressor selection chart] are used to work out C.O.P of each refrigeration system. Density of water, icecream mix and frozen icecream is taken as 1, 3.31 and 2.72kJ/kg.K respectively. Table 2(a) and 2(b) shows the calculation of existing and modified system respectively to manufacture 2000 L/day icecream.

Table 2(a). Electric energy requirement of existing plant

Equipment	Rating (kW)	Multiplication factor	Load factor	Load (kW)	Runtime (hr)	Total load (kWh)
Pasteurization	16.70	1:1	-	16.70	3	50.1
Water heating (Cleaning)	17.41	1:1	-	17.41	4	69.64
Homogenizer	3.75	1:1	0.8	3	2	6
Glycol compressor	18.2*	1:2.64 **	-	6.89	2	13.78
Aging compressor (Aging)	5.02*	1:1.92 **	-	2.61	2	5.22
Aging compressor (Storage)	0.44*	1:1.92 **	-	0.22	18	4.12
Continues freezer Compressor	12.15*	1:1.62 **	-	7.5	5.5	41.25

Continues freezer dasher	3.75	1:1	0.8	3	5.5	16.5
Continues freezer mix pump	0.75	1:1	0.8	0.6	5.5	3.3
Mix Pump	0.75	1:1	0.8	0.6	2	1.2
Pump-1	0.75	1:1	0.8	0.6	7.5	4.5
Pump-2	0.75	1:1	0.8	0.6	2	1.2
Pasteurizer Agitator	0.37	1:1	0.8	0.3	4	1.2
Aging Vat Agitator	0.36	1:1	0.8	0.28	20	5.6
Cooling tower fan motor	0.27	1:1	0.8	0.21	7.5	1.62
Aging condenser fan	0.27	1:1	0.8	0.21	18	3.88
Exhaust fan	2.25	1:1	0.8	1.8	10	18
Fresh air fan	3.75	1:1	0.8	3	10	30
Total						277.11

Table 2(b). Electric energy requirement of modified plant

Equipment	Rating (kW)	Multiplication factor	Load factor	Load (kW)	Runtime (hr)	Total load (kWh)
Electric heater	18.11	1:1	-	-	0.66	11.95
Heat pump	12.36*	1:2.32 **	-	5.32	7.5	39.9
Homogenizer	3.75	1:1	0.8	3	2	6
Glycol PHE compressor	5.35*	1:1.73 **	-	3.09	2	6.18
Glycol aging compressor (Aging)	5.48*	1:1.73 **	-	3.16	2	6.32
Glycol aging compressor (Storage)	0.44*	1:1.73 **	-	0.25	18	4.5
Continues freezer compressor	12.15*	1:1.62 **	-	7.5	5.5	41.25
Continues freezer dasher	3.75	1:1	0.8	3	5.5	16.5
Continues freezer mix pump	0.75	1:1	0.8	0.6	5.5	3.3
Mix Pump	0.75	1:1	0.8	0.6	2	1.2
Pump-1	0.75	1:1	0.8	0.6	2	1.2
Pump-2	0.75	1:1	0.8	0.6	7.5	4.5
Pump-3	0.37	1:1	0.8	0.3	7.5	2.25
Pump-4	0.75	1:1	0.8	0.6	7.5	4.5
Pump-5	0.37	1:1	0.8	0.3	20	6
Pump-6	0.75	1:1	0.8	0.6	7.5	4.5
Pasteurizer Agitator	0.37	1:1	0.8	0.3	4	1.2
Aging Vat Agitator	0.36	1:1	0.8	0.28	20	5.6
Glycol condenser fan	0.27	1:1	0.8	0.21	20	4.32
Exhaust fan	1.5	1:1	0.8	1.2	10	12
Total						183.17

*Refrigeration kW

**C.O.P of refrigeration system

2 ECONOMIC ANALYSIS OF 500L/HR CAPACITY ICECREAM MIX PLANT – A CASE STUDY:

By comparing Table 2(a) and Table 2(b), it has been found that total saving of energy in modified system is 93.94 kWh. By comparing Fig.2 (a) and Fig.2 (b) it is seen that the modified system has additional equipments like heat pump, 4 insulated tanks and additional 4 water pumps while cooling tower is eliminated. Parameters are considered in economic analysis has been given in Table 3.

Table 3. Parameter for icecream plant

Items	Rating
Capacity of icecream mix plant (Liter/hr)	500
Capacity of icecream production (Liter/Day)	2000
Electricity used in existing plant (kWh)	277.11
Electricity used in modified plant (kWh)	183.17
Electricity saved (kWh/Day)	93.94
Rate of electricity (Rs/kWh)	8
Assumed working days	250
Total saving in electricity (Rs)	1,87,880
Cost of additional equipments (Rs)	4,12,000
Additional cost for maintenance (Rs)	20,600
Total saving (Rs)	1,67,280
Life of system (Year)	10
Discount rated (%)	20
Depreciation (%)	10

4 RESULT AND DISCUSSION:

Based on parameters discussed above the following factors are calculated and shown in Table-4 [Motwani K.H., Jain S.V., Patel R.N]. Each factor plays an important role in judging the viability of the project. Internal rate of return is coming as 38% which is more than assumed discount rate 20%. Hence modified project is techno-economically viable.

Table 4. Economic analysis of 500 liter/hr plant

Sr no.	Factor	Value
1	% Saving in Energy	33.8
2	Simple payback period (Year)	2.46
3	Net present value (Rs)	2,89,316
4	Annual life cycle cost (Rs)	1,18,871
5	Life cycle cost (Rs)	4,98,364
6	Depreciation amount (Rs)	41,200
7	Revised investment cost (Rs)	3,70,800
8	Revised net present value (Rs)	4,95,316
9	Revised simple payback period (Year)	2.21
10	Benefit to cost ratio	2.12
11	Internal rate of return (%)	38

REFERENCES:

- Danfoss commercial compressor selection chart, www.commercialcompressors.danfoss.com
 Motwani K.H., Jain S.V., Patel R.N., 2012, Cost Analysis of Pump As Turbine for Pico Hydropower Plants-a Case Study, NUI CONE
 Soylemez M.S., 2005, Optimum heat pump in milk pasteurizing for dairy, Journal of Food Engineering, Volume 74546-551.
 Ubbels J., Bouman S., The saving of energy when cooling milk and heating water on farms, International Journal of Refrigeration, Volume 2, Issue 1, January 1979, 11-16.
 Zaidi A.H., Rawal S.R., Sarma S.C., 1979, Applications of Heat Pump in Dairy Industries, Indian Dairyman, Volume 31, Issue 5303-309.

Surface roughness analysis of piston assembly of ci engine fuelled with diesel, bio-diesel and di ethyl ether (dee) during long term endurance test.

Paresh D Patel

Research scholar, Nirma University Ahmedabad, 328481 Gujarat, India

Rajesh N Patel

Professor and Head of Department, Nirma University Ahmedabad, 328481 Gujarat, India

Sajan Chourasia

Research scholar, Nirma University Ahmedabad, 328481 Gujarat, India

A.M. Lakdawala

Institute of Technology Nirma University, Ahmedabad, Gujarat, India

ABSTRACT:

The current work is extension of our earlier experimental work, based on which, a 20% (v/v) and a 4% (v/v) mixture of Jetropha biodiesel and di-ethyl ether in diesel (B20A4) was established as an optimum bio-diesel fuel blend. The Current experimental research is targeted to inspect the influence of bio-diesel and oxygenated fuel on wear of various components of diesel engine. A long term endurance test is carried out as per IS 10000 (part IX) on a DI diesel engine with B20A4. Test is done under scheduled loading cycles in two stages: engine fuelled with mineral diesel (B0) and engine fuelled with B20A4. After accomplishment of these tests, both the engines are disassembled for detecting the physical surface roughness of various key components of engine, e.g., piston, piston rings, cylinder liner. Surface roughness measurements of these key components are also done to evaluate the wear of these components. The wear of different component except compression ring are found to be lower in the case of B20A4 fuelled engine. To enumerate the wear of engine components, surface roughness at different positions are measured and compared. A qualitative analysis is also carried out by conducting surface profile test and metallurgical microscopy at the same locations.

Keywords: CI Engine, Bio diesel, Di-ethyl Ether (DEE), Life Cycle Analysis, Wear Analysis.

1 INTRODUCTION

Although combustion-associated properties of plant oils are similar to that of mineral diesel oil, the pure plant oils or their mixtures with diesel pose many long-standing problems in CI engines, e.g., Poor atomization characteristics, ring-sticking, injector-choking, injector deposits, injector pump disappointment, and lubricating oil thinning by crank-case polymerization. Such difficulties do not rise with short-range engine operations. Occasionally, the engine fails terribly while operated on pure vegetable oils continuously for an extended period. Hence, the main motivation to carry out the life cycle analysis of CI engine is to analyze and compare wear of vital parts of CI engine like Cylinder Liner, Piston, Pistons Rings, Crank shaft, Crank shaft bearing and journals etc. for a long-term utilization of Bio-diesel or Diesel-Bio-diesel blend. Moreover, the comparison of long term wear of an engine fueled with diesel – biodiesel blended to that with an engine fueled with mineral diesel reveals modifications required to be made in existing CI engine for effective utilization of diesel – biodiesel blend.

According to IS 10000, 1980 for life cycle analysis of internal combustion engine the test engine should be completely dismantled and examined physically so that design features and also the condition of various parts is to be noted before the tests are commenced. After the physical examination, the dimensions of the main moving parts should be checked and recorded in the performance charts in terms of wear. Some of the vital parts are Cylinder Liner, Piston and Pistons Rings. After completion of the initial performance test and physical examination, the engine should be

run for 32 cycles (each of 16 hours continuous running) at the rated speed. The test should be carried out for two different CI engines - one fuelled with Diesel and second fuelled with optimize blend. At the completion of the recommended tests, the engine should be again dismantled. The condition should be noted and the dimensions of critical parts should be recorded in performance chart. The wear of critical components should be recorded in performance chart and should be compared with the declaration made by manufacturer [IS 10000 - V 3].

2 EXPERIMENTAL SETUP AND METHODOLOGY

The experimentations is carried out on computerize test rig equipped with single Cylinder, Kirlosker 4 Stroke, Water cooled, direct injection diesel engine. The test rig is coupled with eddy current dynamometer, crank angle encoder, rota meter and fuel tank with digital piezo sensor, temperature and pressure sensors etc. The setup enables study of VCR engine performance parameters like brake power, frictional power, BMEP, brake thermal efficiency, indicated thermal efficiency, specific fuel consumption, mechanical efficiency, volumetric efficiency, A/F ratio, heat balance and combustion analysis at different values of compression ratio, injection timing and injection pressure. The schematic diagram of experimental setup is shown in Fig. 1 and its specification is provided in Table. 3.

Based on the earlier experimental work conducted for performance and emission, investigations at full fuel delivery settings and different engine load, a 20% blend of jatropha bio-diesel with 4% di-ethyl ether (B20A4) was found to be optimum blend (superior thermal efficiency and lower emission) and selected for long-term endurance test in the current work. The long-term engine endurance experiments is conducted in two phases. In the first phase, the engine is run with diesel (B0) and in the second phase, the engine is run with B20A4. The engines are initially dismantled for physical inspection. After physical examination, dimensions and weight of various parts such as cylinder bore/liners, pistons, and piston rings are recorded. Further, the engines are subjected to 49 hours duration preliminary run before commencing the endurance test. This is done according to test procedure given in IS: 10000 part V, 1980 [IS 10000-V]. The cycle for preliminary test is shown in Table. 1. After a preliminary run, the lubricating oil from the sump is drained off and the engines are refilled with fresh lubricating oil (SAE 20W40), as specified by the manufacturer.

The endurance test is performed as per Indian standard code (IS: 10000 Part IX, 1980) [IS 10000-IX]. The test is conducted for a total of 512 hour duration and consists of 32 nonstop running cycles of 16 hours duration as shown in Table. 2. The lubricating oil samples is collected from the engine after every 128 hour for wear analysis. After conducting the endurance test for the first phase, the engine is dismantled and the physical condition of various engine components is inspected carefully. Moreover, the surface roughness measurement and its microscopic surface images is also inspected. For the second phase of life cycle analysis, a new engine is installed on the same test rig and fuelled with B20A4. The above mentioned procedure, i.e., preliminary runs, endurance test, lubricating oil collection, and wear measurement are followed for second phase (B20A4) also.

Note that the surface roughness profiles of various engine components is measured using stylus based surface roughness meter (Maker: CARL-ZEISS, Specification: Minimum display value 0.01 μm , Accuracy: CLASS 1 (DIN 4777)) while for the wear analysis metallurgical microscopy is used. The magnification used in the said microscope is 50X and 1000X [Sinha Shailendra Agarwal, Kumar, 2010, A. K. Agarwal J. Bijwe L. M. Das Bora Dilip Kumar L M Das and M K G Babu].

Table 1. Loading cycle for preliminary runs for constant speed diesel engine, showing load (% of rated load) VS running time (hour) provided by IS 10000 Part - V, 1980 [2]. The cycle is shown for 7 hours. Seven such cycle is carried out for 49 hours preliminary runs.

Load (% of rated load)	Running time (Hours)
25	1.5
50	2
75	1.5
100	2

Table 2. Loading cycle for long - term endurance test for constant speed diesel engine, showing load (% of rated load)VS running time (hour) including warm up period provided by IS 10000 Part - IX, 1980 [2].

Load (% of rated load)	Running time (Hours)
100 (Including warm up)	4
50	4
110	1
No load (Idling)	0.5
100	3
50	3.5

Table. 3 Engine Specifications.

Components	Specification
Engine	Research Engine test setup 1 cylinder, 4 stroke, Multi fuel (Computerized), Water cooled, STROKE 110mm, BORE 87.5mm
Diesel mode	Power 3.5 kW C.R. range 12.1-18.1 Speed 1500 rpm Injection Variation 0-250 BTDC
Compression ratio	18:1
Inlet valve open BTDC	15 Degree
Injection start BTDC	20 Degree
Inlet valve close ABDC	30 Degree
Exhaust Valve Open BBDC	30 Degree
Exhaust Valve close ATDC	15 Degree
Fuel injection Pressure	180 Bar
Dynamometer	Eddy current type, water cooled, with loading unit
Fuel tank	Capacity 15 lit, Type: Duel compartment, with fuel metering pipe of glass
Air box	M S fabricated with orifice meter and manometer
Calorimeter	Type Pipe in Pipe
Rota meter	Engine cooling 40-400 LPH , Calorimeter 25-250 LPH
Piezo sensor	Combustion: Range 5000 PSI, with low noise cable Diesel line: Range 5000 PSI, with low noise cable
Crank Angle Sensor	Resolution 1 Degree, speed 5500 rpm with TDC pulse
Temperature Sensor	Type RTD,PT100 and Thermocouple
Load Sensor	TYPE K Load cell, type strain gauge, range 0-50 Kg
Fuel Tank	Capacity 15 LIT
Fuel flow transmitter	DP transmitter, Range 0-500 mm WC
Software	ENGINESOFT, engine exhaust performance analysis software
Rota meter	Engine cooling 40-400 LPH; Calorimeter 25-250 LPH
Data acquisition device	NI USB-6210, 16-bit, 250kS/s
Digital voltmeter	Range 0-20V, panel mounted
Air flow transmitter	Pressure transmitter, Range (-) 250 mm WC
Pump	Type , Monoblock
Overall dimensions	W 2000 x D 2500 x H 1500 mm

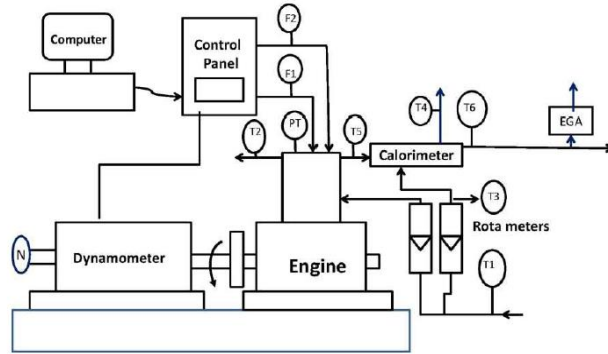


Figure 1. Line diagram of the experimental setup used in the present study. T1 - inlet (engine) water temperature (°C), T2 - outlet (engine) water temperature (°C), T3 - inlet (calorimeter) water temperature (°C), T4 - outlet (calorimeter) water temperature (°C), T5 - exhaust gas temperature before calorimeter (°C), T6 - exhaust gas temperature after calorimeter (°C), F1 & F2 - fuel consumption and air flow measurement, PT - Pressure transducer, EGA - exhaust gas analyser and N - engine speed measurement.

Component	Diesel		B20A4		Roughness Plot	
	Microscopic Image	Ra & Rq (µm)	Microscopic Image	Ra & Rq (µm)		
Piston Top	50 X	Ra = 1.180	50 X	Ra = 1.00	+ 20.1	Diesel
	1000 X	Rq = 1.490	1000 X	Rq = 0.960	- 20.1	
Compression Ring	50 X	Ra = 0.940	50 X	Ra = 1.500	+ 21.3	B20A4
	1000 X	Rq = 1.150	1000 X	Rq = 2.00	- 21.3	
Cylinder Liner	50 X	Ra = 0.710	50 X	Ra = 0.740	+ 22.5	Diesel
	1000 X	Rq = 1.010	1000 X	Rq = 0.960	- 22.5	
				+ 25	B20A4	
				- 25		
				+ 10.8	Diesel	
				- 10.8		
				+ 15	B20A4	
				- 15		

Figure 2 Microscopic and surface roughness analysis of CI engine components including piston, nozzle tip, inlet valve, exhaust valve, cylinder head, crank shaft bearing and cylinder liner. Figure shows the comparison between diesel and B20A4 fuelled engine components microscopic surface image taken at 50X and 1000X magnification along with that the surface roughness measurement data including Ra and Rq value were shown with their roughness plot.

3 RESULTS AND DISCUSSION

Fig. 2 shows the comparison of surface roughness and close microscopic image analysis of two fresh engine components fuelled with diesel and optimum blend B20A4. The surface roughness is measured with ISO 97/JIS 01 standard at IGTR. In the case of piston top it shows the lower Ra and Rq value for B20A4 compare to diesel. Note that the Ra and Rq values are the average and root mean square values of surface roughness measured with ISO 97/JIS 01. Moreover, in microscopic image

taken at 50X and 1000X magnification with metallurgical microscope, it is clearly visible that the wear found to be quite high with diesel as compared to B20A4. Further, in the case of compression ring it is found that the Ra and Rq values are higher and also the microscopic image for surface roughness are found to be slightly rough in B20A4 as compared to diesel. For the case of cylinder liner it is observed that the Ra and Rq values are almost similar in both case of B20A4 and diesel. From the qualitative assessment shown in Fig. 2 it is concluded that in over all cases the surface roughness of diesel fuelled engine is found to be more as compared to its counterpart of B20A4.

The reasons for more surface roughness and more wear in diesel compare to B20A4 is as follows: The compression ring belt region, with the top area and the piston ring, is straight thermally exposed with the combustion hot gases and hence it is subjected to temperature changes. The peak temperatures of gases inside the combustion chamber during combustion in a CI engine fuelled with diesel can increase to nearly 2500°C. Great heat fluctuation causes difficulties such as thermal stress with reduction of the lubricating oil film in between parts. Due to high combustion temperature difference on piston top area reduces the hardness of the piston. Furthermore, as the temperature rises, the yield strength and shear strength of material reduces. However, in the case of B20A4 the combustion temperature cannot reach to such a high value as in case of diesel. This is due to the fact that the calorific value of B20A4 is lower as compared to diesel. At the same time B20A4 contains 20% v/v of bio-diesel which has self-lubricating properties – in turn reduces the amount of wear and roughness [Andersson,2002].

4. CONCLUSION

An endurance test is carried out on the DI engine with Jatropha bio-diesel and additive di-ethyl ether to see its viability as a substitute for mineral diesel. The wear pattern of surfaces of various components is analysed. A low wear is observed for the piston for B20A4. Surface roughness profiles, various roughness parameters, and microscopic image show that wear is relatively higher at the crank shaft bearing and inlet valve with B20A4 but overall wear is lower than diesel fuelled engine. A long-term endurance test conclusively proves that bio-diesel can be successfully used for partial substitution of mineral diesel. It can also be concluded that bio-diesel can readily be adopted as an alternative fuel in the existing DI engines without any major modifications in the engine hardware.

ACKNOWLEDGEMENT

The authors are sincerely acknowledge the financial support received from Gujarat Council on Science and technology (GUJCOST), Gandhinagar, Gujarat, India for the Minor Research Project entitled “An Experimental Investigation on Life cycle Analysis and Combustion Characteristics of CI Engine operating on Esterified oil and its blends with bio Additives” wide letter No. GUJCOST/MRP/2014-15/392, Dated 30/06/2014.

REFERENCES

- A. K. Agarwal, J. Bijwe, L. M. Das. Effect , April 2003 , of Bio-diesel utilization of wear of vital parts in Compression Ignition Engine Transaction of ASME vol 125603-611
- Bora, Dilip Kumar, L M Das and M K G Babu., , Aug 2010, Wear and tear analysis of a single cylinder diesel using karanja bio-diesel (B20) after 512 hours, Journal of Scientific & Industrial Research, Vol 69pp. 639-642.
- Bureau of Indian Standard: 10000: Part V.
- Bureau of Indian Standard: 10000: Part IX.
- Peter Andersson, Piston ring tribology A literature survey, Jaana Tamminen & Carl-Erik Sandström Helsinki University of Technology, 2002 , Internal Combustion Engine Laboratory
- Sinha, Shailendra, Agarwal, Avinash Kumar., 2010, Experimental Investigation of the Effect of Bio-diesel Utilization on Lubricating Oil Degradation and Wear of a Transportation CIDI Engine, Journal of Engineering for Gas Turbines and Power, ASME, Vol. 132/ 042801-1.

Numerical analysis on effect of baffle inclination angle on flow and heat transfer characteristic of shell and tube heat exchanger with helical baffle

Unnat Prajapati

Junior Engineer, Heat Chem Engineers Pvt. Ltd., Ahmedabad, Gujarat, India

Absar Lakdawala

Associate Professor, Mechanical Dept, Institute of Technology, Nirma University, Ahmedabad, Gujarat, India

ABSTRACT: In the present work numerical simulation is done to show effect of baffle inclination angle on thermal and hydraulic performance of shell and tube heat exchanger. For the said analysis a geometric similar model with 09 circular tubes in line arrangement is considered. The CAD model of the same is created using an unstructured Tetra/Hybrid mesh. Using finite volume method, steady flow momentum and energy equation are solved. Moreover, Renormalization Group (RNG) $k-\epsilon$ is selected for the turbulent modeling. Simulations are carried out for ten different Reynolds number ranging $400 \leq Re \leq 2200$; three different Prandtl number between $0.7 \leq Pr \leq 118.2$ and four different baffle angle between $20^\circ \leq \theta_b \leq 50^\circ$. The methodology is validated with published experimental results and found to be in good agreement. The results shows that, shell and tube heat exchanger with helical baffle producing more vortex flow and hence have higher heat transfer co-efficient and lower pressure drop as compared to the segmental baffle. The simulation results shows that 40° helical baffle has 76.35% higher heat transfer co-efficient per unit pressure drop (Nu/f) as compare to segmental baffle heat exchanger.

Keywords: Helical baffle, Numerical analysis, $k-\epsilon$ model, Thermo-hydraulic performance

1. INTRODUCTION

In most of the industries shell and tube heat exchanger is used with segmental baffle plate on the shell side. However, it should be noted that the segmental baffle plate have few adverse effects - more pressure drop, higher fouling and higher maintenance cost - on thermo-hydraulic performance of heat exchanger. The problems can be minimized with the use of helical baffle instead of segmental baffle. The effect of baffle inclination angle on fluid and heat transfer of heat exchanger using numerical methodology was carried out by [Lei Y. G. et al]. They showed that due to elimination of dead zone in continuous baffle heat exchanger, the pressure drop found considerably lower as compared to segmental baffle. Moreover, it was shown that although the heat transfer co-efficient is lower in case of helix heat exchanger, the heat transfer per pressure drop is found superior as compared to segmental baffle. Chen et al. showed numerically the formation of circulation and rotating spiral flow - called as secondary flow on the shell side. The phenomenon enhances the heat transfer of heat exchanger [Chen Y. P., Sheng Y. J., Dong C., Wu J. F]. Through the numerical investigation [Lei Y. G. et al, Xiao X. et al, Zhang J. F. et al] showed that 40° helical angle is found to be the best selection for improvement in thermo-hydraulic performance. Moreover, 40° helical baffle is no more the best selection if the Prandtl number of the fluid on the shell side is higher. When Prandtl number is large enough, heat exchanger with small helical angle reveals to be the optimal choice [Xiao X. et al]. The experimental test are performed on several shell-and-tube heat exchangers, with segmental baffles as well as with helical baffles at helix angles of $20^\circ \leq \theta_b \leq 50^\circ$. Nusselt number (Nu) and friction factor (f) correlations are obtained at helical angle $20^\circ, 30^\circ, 40^\circ$ and 50° [Zhang J. F. et al, Zhang J. F. et al].

2. COMPUTATIONAL MODEL AND NUMERICAL METHOD

2.1 Computational model

The present study aims to numerically investigate flow in helical baffle heat exchanger. The computational domain with continues helical baffle at 40° of baffle angle is shown in Fig. 1 representing side view and front view. Geometry parameters considered in the present study are shown in Table 1.

2.2 Governing equation and Boundary Condition

Three-dimensional fluid motions in continues helical baffle shell and tube heat exchanger can be solved by mathematical modeling and numerical implementation for the fluid region.

Mass Conservation (Continuity) Equation:

$$\frac{\partial}{\partial x_i}(\rho u_i) = 0$$

Momentum Conservation Equation:

$$\frac{\partial}{\partial x_i}(\rho u_i u_k) = \frac{\partial}{\partial x_j} \left(\mu \frac{\partial u_k}{\partial x_i} \right) - \left(\frac{\partial P}{\partial x_k} \right)$$

Energy Conservation Equation:

$$\frac{\partial}{\partial x_i}(\rho u_i t) = \frac{\partial}{\partial x_i} \left(\frac{k}{C_p} \frac{\partial t}{\partial x_i} \right)$$

Inlet velocity of fluid is taken according to the Reynolds number range from $400 \leq Re \leq 2200$. Pressure boundary condition is used at the outlet and set 0 gauge pressure. The fluid inlet temperature is set to be 335 K. The working fluids are air ($Pr=0.74$), water ($Pr=6.99$) and oil ($Pr=118.2$). Adiabatic boundary conditions are set at the shell wall and the baffle plate, and the no-slip boundary condition is applied at the impermeable heat exchanger tubes, shell wall and baffle plate. Over the tube the dimensionless length y^+ is $0.30 < y^+ < 3.0$. The tube wall temperature is set to be 300 K and the properties of the fluid and the solid wall are constant.

Table 1 Geometry Parameter

Parameter	Value
Tube Pitch	0.025
Number of Tubes	09
Shell Diameter	0.110
Tube outside diameter	0.019
Effective length of tube	1
Tube layout pattern	90°
Tube pass	1
Baffles angle	$20^\circ, 30^\circ, 40^\circ, 50^\circ$
Baffle spacing	0.02743-0.18535

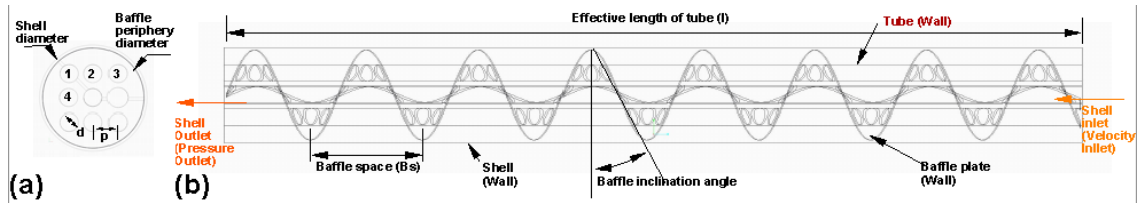


Fig. 1 Schematic diagram (a) side view with flow parameter (b) front view

2.3 Grid Generation and Numerical Solution

The computational domain is discretized (grid generation) by the commercial code Ansys mesh. The domain is meshed with unstructured Tet/Hybrid with default scheme. Due to complexity of the present computational domain, the grid is

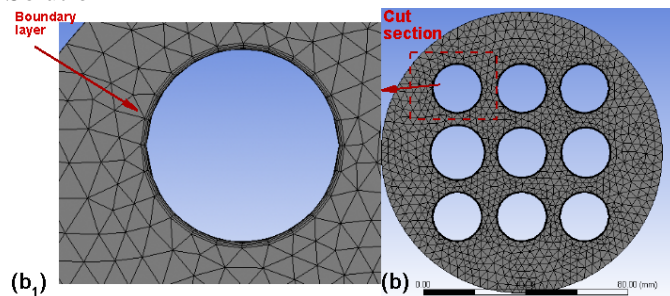


Fig. 2 Grid of the configuration (b) side view (b1) grid generated over Tubes

generated with a boundary layer over each tube. Grid elements considered for simulation work at different baffle angles are 2831868 to 2750688. Side view of the geometry with grid generation of shell and tube heat exchanger with continues helical baffle at 40° of helix angle is shown in Fig. 2. The Fig. 2b₁ shows the exploded view of boundary layer generated over tubes.

The computer code FLUENT 6.3 is used to solve - Steady State - fluid flow and heat transfer equations in the computational domain. Pressure base solver is selected. For the turbulence modeling $k-\varepsilon$ is selected for the swirl flow on shell side to enhance the simulation accuracy. The governing equations are iteratively solved by the finite volume method using SIMPLE pressure-velocity decoupling algorithm. The convective terms in Momentum, Turbulent kinetic energy and Turbulent dissipation governing equations is discredited by the QUICK scheme. The under relaxation factor are set to be 0.3, 0.7 and 1 for pressure, momentum and energy respectively. The convergence criteria considered to be 10^{-3} for the flow equations and 10^{-6} for the energy equation.

2.4 Parameter Reduction

For the calculation of various governing and engineering important parameters of helical heat exchanger, following methodology is adopted.

Transverse area: It is area from where the shell side fluid is flowing

$$S = \frac{1}{2} B D_s \left(1 - \frac{D_{to}}{P_t} \right) \quad \text{Where, B (Baffle spacing) in equation is given as: } B = \sqrt{2} D_s \tan \theta_b$$

The Reynolds number of the shell side fluid flow is calculated as:

$$Re = \frac{\rho D_e u}{\mu} \quad D_e \text{ is equivalent diameter taken as tube outer diameter } d_{to},$$

LMTD of heat exchanger:

$$\Delta T_{LMTD} = \frac{(Th_i - T_w) - (Th_o - T_w)}{\ln \left(\frac{Th_i - T_w}{Th_o - T_w} \right)}$$

Frictional factor:

$$f = \frac{1}{4} \left(\frac{\Delta P}{\frac{1}{2} \rho u^2} \frac{D_e}{L} \right)$$

3. MODEL VALIDATION

In order to verify the results of simulation model, a comparisons of present numerical results are done with the experimental results of [Zhang J. F. et al]. Simulation model is validated with experimental results for heat exchanger having 30° of baffles angle and $100 \leq Re \leq 700$ as shown in the Fig. 3. As per the Bell-Delaware methodology, the shell side flow can be divided into five different stream [Kakac,2002]. In CFD simulations the bypass streams in the tube bundle and leakages are neglected. Moreover, in experiment setup due to manufacturing limitations there exist tolerance and fits. Due to this results are deviating. The minimum and maximum deviation between present numerical and published experimental [Zhang J. F. et al] values of $Nu/Pr^{1/3}$ is found to be 2.83-33.50%.

4. RESULT AND DISCUSSION

In order to understand the effect of baffle angle on thermal and hydraulic performance of shell and tube heat exchanger, 130 cases are simulated.

4.1 Shell Side Velocity and Vorticity Distribution

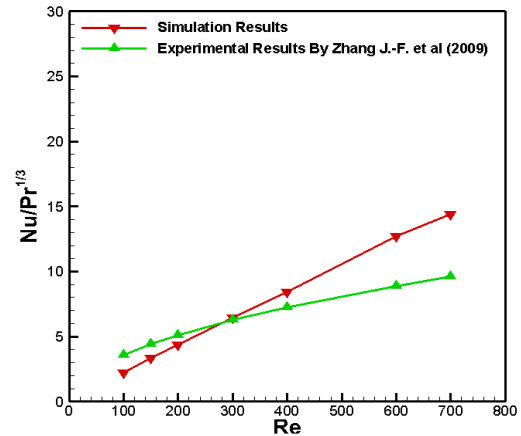


Fig. 3 Comparison between experimental and simulation results represents at 30° inclination of baffle

Figure 4a and d illustrates contours of the velocity magnitude in longitudinal section plane with $Re=2200$ and $Pr=6.99$ of segmental baffle and 40° baffle angle heat exchanger. The velocity magnitude is higher and uniform in the active zone as compared to in the dead zone. The velocity magnitude is nearly equal to 0.4 for segmental baffle on the other hand the velocity magnitude is decreasing to 0.17 for 40° of helical baffle. For segmental baffle the velocity

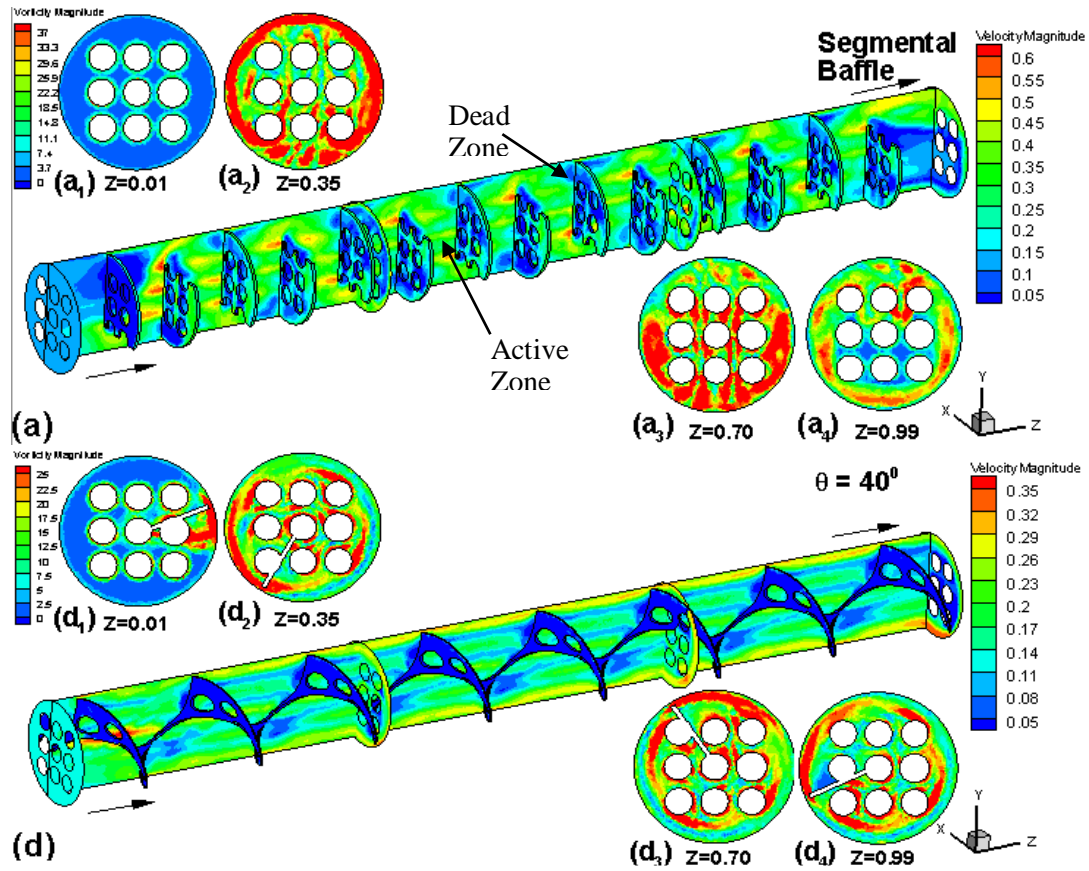


Fig. 4 Contours of the velocity magnitude in longitudinal section plane and vorticity magnitude in transverse plan (a) Segmental baffle (d) $\theta_b=40^\circ$

distribution is not uniform near the baffle plate whereas the velocity distribution is uniform near the baffle for helical baffle plate. The entering and exit velocities of segmental baffle are low as compare to the flow velocity whereas velocity remains uniform through for helical baffle.

In Fig. 4a four transverse plane a_1 to a_4 represents vorticity magnitude at distance of 0.01 m, 0.35 m, 0.70 m and 0.99 m respectively. At $Z=0.01$ m vorticity magnitude is higher over the tube segment and low and uniform at other places. As the distance increases from $Z=0.01$ to $Z=0.35$ m the vorticity is higher near the periphery of shell wall and non-uniform at other places. Now as the distance increasing vorticity decreasing non-uniformly. For 40° helical baffle vorticity is uniform over the periphery of shell wall. Moreover it should be note that 40° helical baffle vorticity is uniform along the distance.

4.2 Shell Side Temperature Distribution

Figure 5 shows the contour of temperature distribution along the longitudinal direction with $Re=2200$ and $Pr=6.99$ for Segmental baffle and helical

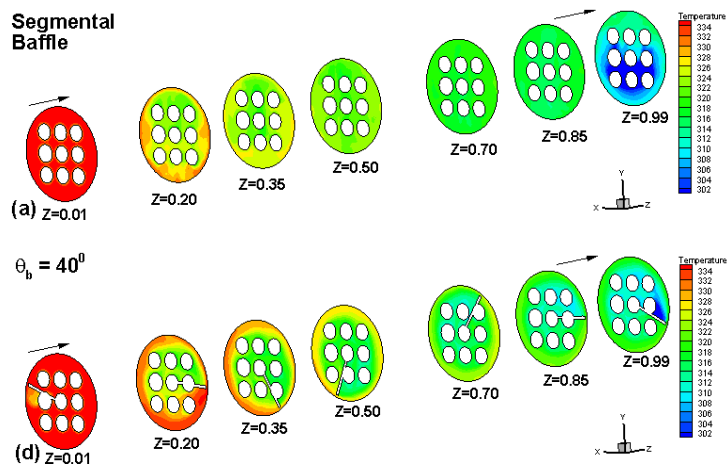


Fig. 5 Contour of temperature distribution in longitudinal section plane along the distance (a) segmental baffle (d) $\theta_b=40^\circ$

baffle. The shell-side flowing fluid temperature rises steadily and uniformly along the shell. For helical baffle heat exchanger as the baffle angle increases the temperature is consistently rises in three meridian planar sections. The temperature is higher near periphery than near the axis throughout the shell. The temperature gradient is apparently sharper in the area around the tube wall than in other regions.

4.3 Comprehensive Performance Analysis

The ratio of Nusselt number and frictional factor (Nu/f) illustrated in the Fig. 6. The analysis results show that the ratio of non-dimensional parameter is increased with helical angle. Baffle angle of 40° and 50° have higher value as compared to segmental baffle at same Reynolds number. From Figures 6b₁, b₂ and b₃, it is evident that the ratio Nu/f on shell side for 40° and 50° of helical angles are 66.34-76.35% and 79.72-87.34% respectively higher as compared to segmental baffle. For $Pr=6.99$ the comparison made between segmental baffle and helical baffle for Nu/f ratio shows that the difference is not significant for 20° helical baffle than segmental baffle. It is observed that the difference in the ratio of Nu/f between 20° helical baffle than

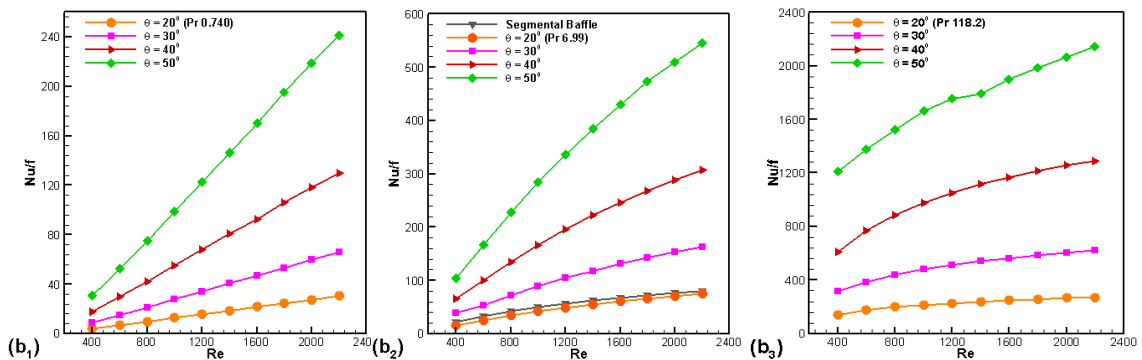


Fig. 6 Reynolds number vs Nusselt number/Frictional Factor (b₁) Air ($Pr=0.74$) (b₂) Water ($Pr=6.99$) (b₃) Oil ($Pr=118.2$)

segmental baffle is not significant for all Pr simulated in the present work.

5. CONCLUSION

For varying Reynolds number the percentage difference of heat transfer co-efficient increase with lower Prandtl Number and higher Baffle angle. Similarly for varying Reynolds number the percentage difference of pressure drop per unit length increase with higher Prandtl Number and lower Baffle angle. Shell and tube heat exchanger with helical baffle have lower heat transfer co-efficient and pressure drop than segmental baffle. The non-dimensional parameter at 40° and 50° of helical baffle have higher performance than segmental baffle. However, the effects of inclination angle on pressure drop and frictional factor on shell side are small when $\theta_b=40^\circ$.

REFERENCES

- Chen Y. P., Sheng Y. J., Dong C., Wu J. F., 2013, Numerical simulation on flow field in circumferential overlap trisection helical baffle heat exchanger. *App. Therm. Engg.* Vol. 50, 1035-1043
- Heat Exchangers by Sadik Kakac, 2002, Selection Rating and Thermal Design
- Lei Y. G. et al., 2008, Effects of baffle inclination angle on flow and heat transfer of a heat exchanger with helical baffles. *Chem. Engg. and Pro.* Vol. 47, 2336-2342
- Xiao X. et al, Numerical investigation of helical baffles heat exchanger with different Prandtl number fluids, 2013, *International Journal of Heat and Mass Transfer* Vol. 63, 434-444
- Zhang J. F. et al., 2009, Experimental performance comparison of shell-side heat transfer for shell-and-tube heat exchangers with middle-overlapped helical baffles and segmental baffles. *Chem. Engg. Sci.* Vol. 64, 1643-1653
- Zhang J. F. et al., 2013, Experimental performance comparison of shell-and-tube oil coolers with overlapped helical baffles and segmental baffles. *App. Therm. Engg.* Vol. 58, 336-343,

Numerical simulation and modelling of downdraft gasifier

Jagdish R. Kanjariya

Department of Mechanical Engineering, Institute of Technology Nirma University, Ahmedabad, Gujarat, India, 382481.

Rajesh N. Patel

Department of Mechanical Engineering, Institute of Technology Nirma University, Ahmedabad, Gujarat, India, 382481.

Absar M. Lakdawala

Department of Mechanical Engineering, Institute of Technology Nirma University, Ahmedabad, Gujarat, India, 382481.

ABSTRACT: In gasification process raw materials reacts with air, oxygen, stem or their mixture to produce syngas. The syngas produced has useful heating values and can be used as fuel for generating heat and power. The gasifier considered in this study is Downdraft throat type, fixed bed, 10 kW downdraft gasifier located at Nirma University's gasifier laboratory. Design data and material grades for modeling were taken from the same gasifier. The objective of this study is to develop a numerical model to investigate the Thermal-hydraulic and gasification process inside a Downdraft gasifier using the commercial CFD solver ANSYS/FLUENT 14.5. Turbulence model selected is standard k- ϵ model and combustion process has been displayed by species transport model to calculate global gasification reaction. In CFD of gasification chemical reactions considered are combustion, gasification, methanation, partial combustion and water gas shift reaction. Radiation model P1 is considered for radiation heat transfer. Discrete phase model is used to consider heat, mass transfer and momentum between solid phase and gas phase. Stochastic particle tracking method is used for considering turbulent dispersion. The influence of variation in fuel composition, calorific value and Equivalence ratio (ER) on temperature distribution in various zone is evaluated. It is observed that with Equivalence ratio 0.25 the outlet temperature is 960 K while that with 0.35 is 1024 K.

Keywords: downdraft gasifier, equivalence ratio, species transport

1 INTRODUCTION

Gasification is a very efficient method for extracting energy from many different types of organic materials. Considering environmental pollution from energy conservation system gasification is near zero pollution technology with high thermal efficiency for syngas production. Gasification is a thermochemical process that converts carbon based material like coal, petroleum, biomass in to gaseous fuel. In gasification, raw materials reacts with air, oxygen, steam or their mixture at temperature higher than 700 °C to produce syngas. The syngas produced has useful heating values and can be used as fuel for generating heat and power. The calorific value of syngas produced is determined by gasifying medium. In gasification process oxygen molecules are less than carbon molecules which indicate that the gasification process operates at limited amount of oxygen. Oxygen is deliberately supplied in less amount so that carbon and hydrogen present in feed stock does not get converted to CO₂ and H₂O respectively. The syngas is a mixture CO, H₂, CH₂, CO₂, N₂ and H₂O out of which CO, H₂ and CH₄ are combustible rest are noncombustible components [T. Reed, A. Das. 1988]. There are four type of gasifiers: 1.fixed bed gasifier 2.fluidized bed gasifier 3. Entrained flow gasifier 4.transport gasifier. The main benefits of fluidized bed gasifiers is, it can be handle practically any coal, synthetic gas produced is free of oils and tars, very high carbon conversion ratio [C. Chen, M. Horio, T. Kojima. 1999].

2 DESIGN AND BOUNDARY CONDITION

This research studies a Downdraft gasifier. The geometry of the gasifier used in the simulation is shown in Fig.1 the geometry and the operating conditions are based on Nirma University laboratory scale gasifier. The gasifier is divided into four regions: drying zone and pyrolysis zone are upper stage of gasifier, combustion zone and reduction zone are lower stage of gasifier. The gasifier has symmetry two injector of the air in combustion region in lower stage of gasifier. All the wood and biomass waste are injected in upper section of the gasifier. Dimension and other parameter are taken similar to Patel et al, [V. Patel, D. Upadhya, R. Patel. 2014.]. The model of gasifier is discretized using unstructured hybrid mesh in ANSYS meshing modeler. The total no of elements used in the present study is nearly 5 lakh.

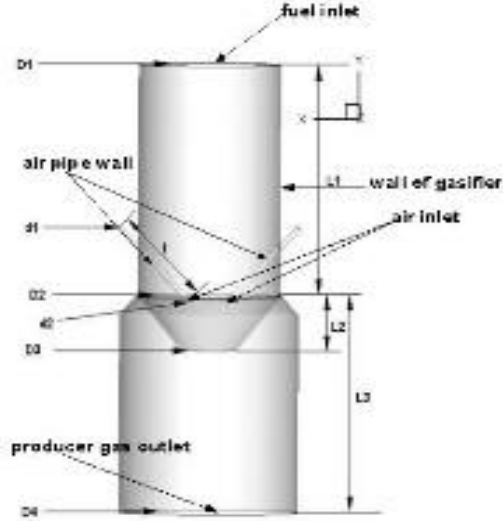


Figure 1 Downdraft gasifier model

Table 1 Dimensions of downdraft gasifier

Name	Dimension(mm)	
D1	Inlet diameter	500
D2	Throat diameter	500
D3	Throat outlet diameter	155
D4	Ash outlet diameter	630
d1	Air inlet diameter	20
d2	Air outlet diameter	20
l	Air pipe length	350
L1	Hopper length	765
L2	Throat length	185
L3	Reduction cell length	661
L	Total length	1426
θ	Throat angle	45°

Boundary Name	mass flow specification	mass flow rate(kg/s)	Temperature (K)	Turbulence method	Turbulence intensity	Hyd. Dia	Em-Isivity
Air inlet	Mass flow rate	0.0046	430	Intensity & hyd. dia	10%	20	-
Air pipe wall	No slip	-	300	-	-	-	0.77
Fuel inlet	Mass flow rate	0.00278	300	Intensity & hyd. dia	10%	500	-
Producer gas outlet	Out flow	-	-	Intensity & hyd. dia	10%	630	-
Wall of gasifier	No slip	-	300	-	-	-	0.77

Table 2 Boundary condition table at 0.25 equivalence ratio

3 GOVERNING EQUATION AND CHMICAL REACTION

The governing equations for continuity, momentum, energy and species transport equation for the fluid region are as follows [A. Silaen, T.Wang. 2010]:

3.1. Mass conservation equation:

$$\frac{\partial}{\partial x_i}(\rho u_i) = S_m \quad (1)$$

Where ρ is density, S_m is source term.

3.2. Momentum conservation equation:

$$\frac{\partial}{\partial x_i}(\rho u_i u_j) = \rho \overline{g_j} - \frac{\partial p}{\partial x_i} - \frac{\partial p}{\partial x_j} + \frac{\partial}{\partial x_i}(\tau_{ij} - \rho \overline{u_i u_j'}) + S_j \quad (2)$$

Where τ is stress tensor.

3.3 Energy conservation equation:

$$\frac{\partial}{\partial x_i}(\rho C_p u_i T) = \frac{\partial}{\partial x_i} \left(\lambda \frac{\partial T}{\partial x_i} - \rho C_p u_i \overline{T'} \right) + \mu \Phi + S_h \quad (3)$$

Where C_p is specific heat, λ is heat conductivity and Φ is viscous dissipation.

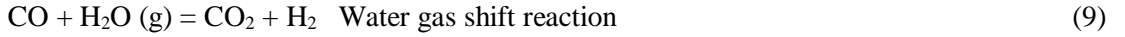
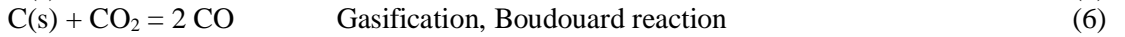
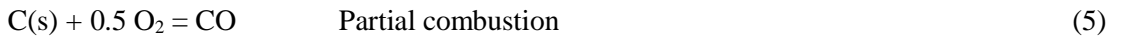
3.4. Species transport equation:

$$\rho \frac{\partial}{\partial x_i}(u_i Y_j) = \frac{\partial}{\partial x_i} \left(D_i \frac{\partial Y_j}{\partial x_i} - u' Y' \right) \quad (4)$$

Where D_i diffusion coefficient and Y is mass fraction of species.

For CFD analysis of gasification process, along with steady state mass, momentum and energy standard k- ϵ model for turbulence modeling and Species transport model for combustion modeling is selected. Moreover, P1 model for radiation modeling, discrete phase model with stochastic particle tracking for coupling between solid phase and gaseous phase are selected.

This study deal with global chemical reaction of wood gasification. The generalized equation are listed as Eq. (5) to (11), In this study water gas shift reaction and methanation chemical reaction are considered.



4 RESULTS AND DISCUSSION

Note that the different equivalence ratios are obtained by varying mass flow rate of air for fixed mass flow rate of fuel. The results obtained from the CFD simulation are discussed here. For the species transport model, the proximate and ultimate analysis of fuel used in the gasifier is required to be given as input parameter. The proximate and ultimate analysis is shown in Table 3 for wood biomass.

Table 3 Ultimate and proximate analysis of wood as well as boundary condition for various mass fraction

Proximate		Ultimate		Oxide	
Volatile Matter	0.8285	Carbon	0.4960	Nitrogen	0.7666
Ash	0.0079	Hydrogen	0.063	Oxygen	0.2333
Moisture	0.0669	Nitrogen	0.004		
Fixed carbon	0.0967	sulfur	0.0002		
		Oxygen	0.04368		

4.1 Flow distribution in gasifier

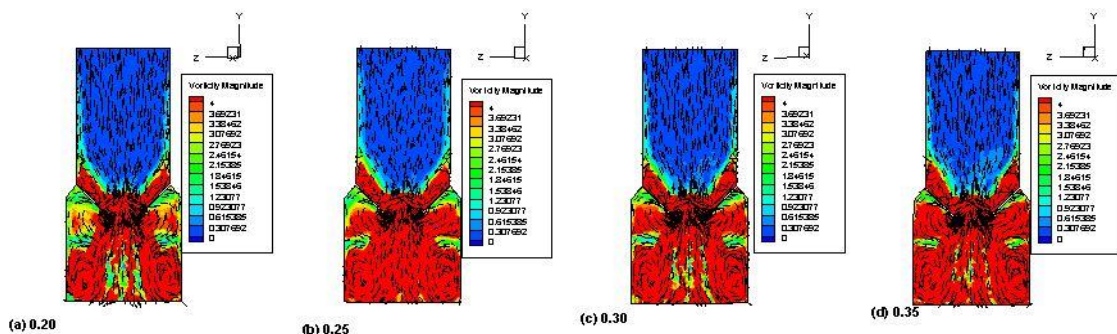


Figure 2 Velocity magnitude in axial direction for down draft gasifier with different equivalent ratio. Here, (a) ER = 0.2 (b) ER = 0.25 (c) ER = 0.30 (d) ER = 0.35

Figure 2 shows variation of velocity magnitude in down draft gasifier for different equivalence ratio. It can be seen in Fig. 2 that the velocity field can be divided in two parts: (1) Passive region (upper part of the gasifier): In this region the velocity magnitude is small and the flow is diverted towards the downward direction. The passive velocity field is a first qualitative indication of pyrolysis and drying zone with lower temperature field. (2) Active region (lower part of gasifier): The active region is seen between air inlet and outlet of gasifier (see Fig. 2 the velocity contours indicated with red color). The formation of vortex is seen in the active region. The formation of vortex is indication of combustion and reduction zone. Moreover, the production of vortex is responsible for transport of H_2 and CO to the lower part of the gasifier. The comparison of vortex at different equivalence ratio (Fig. 2 a, b, c and d) clearly shows that the intensity of vortex increases with equivalence ratio. The increase in vortex strength can be correlates with increase in temperature of combustion zone as equivalence ratio increases.

4.2 Temperature Distribution in Gasifier

Figure 3 shows temperature distribution in to perpendicular planes at mid-section. It can be seen in Fig. 3 and that the upper zone (passive region as discussed in previous section) experiences lower temperature while lower zone (active region) experiences higher temperature indicating pyrolysis for upper and combustion and reduction for lower zone respectively. This can be explained as follows: The heat is absorbed during pyrolysis reaction leading to reduction in temperature while heat release takes place during oxidation reaction which increases the temperature of combustion zone. The maximum temperature observed is around 1280 K near to throat section of gasifier for ER = 0.35. (See Fig.3 (d)). The higher temperature near to throat section is observed due to higher concentration of oxygen leading to combustion. Finally slightly lower temperature as compared to throat section is seen in reduction zone of gasifier. This is because of hot gases are reduced by unreacted char in this zone. Moreover, due to increase in availability of oxygen with increasing ER, the gas temperature is found to be higher (compare temperature distribution in Fig.3 at different ER).

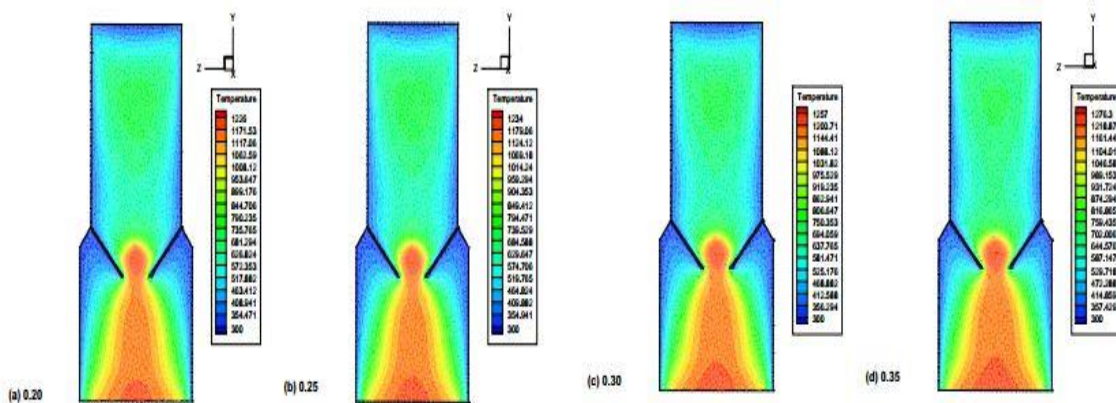


Figure 3 Temperature profile across (X = C) mid plane of downdraft gasifier with different equivalence ratio. Here, (a) ER = 0.20 (b) ER = 0.25 (c) ER = 0.30 (d) ER = 0.35

4.3 Mass fraction concentration

The zone-wise temperature variation in different zone of gasifier at different ER is shown in Fig. 4. The variation of temperature is found to be in good agreement with the theory. Figure 5 illustrates syngas composition for different equivalence ratios of 0.2, 0.25, 0.3, and 0.35. With increasing equivalence ratio, it is observed that the concentration of H_2 decreases, while N_2 increases. This is due to infiltration of more air in the gasifier which brings more nitrogen and oxygen. It is also observed that the mass fraction of hydrogen decreases due to dilution effect. Figure 5 also shows that CO concentration increase first and then decrease viz a viz for CO_2 . The results leads to conclusion that there is an optimal value of equivalence ratio about

0.3 producing best quality of syngas. Due to availability of higher oxygen for complete combustion CH_4 found to be decreases with increase of equivalence ratio.

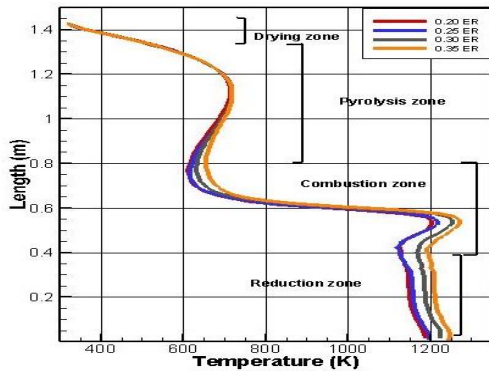


Figure 4 Temperature variation at different equivalence ratio in different zone

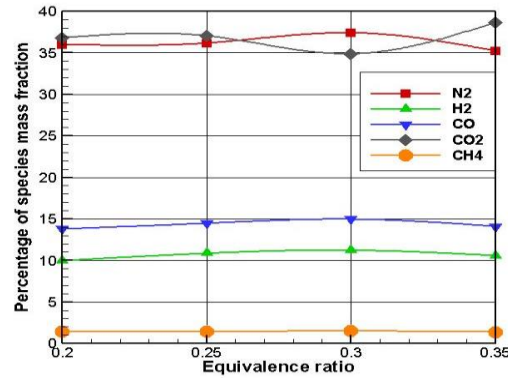


Figure 5 Mass fraction of species at outlet of gasifier

Table 4 Summary

Case No.	Equivalence ratio	Inlet Temp. of Air(K)	Outlet Temp. of syngas (K)	N_2	H_2	CO	CO_2	CH_4
1	0.20	430	928	36	9.97	13.78	36.8	1.47
2	0.25	430	960	36.17	10.85	14.47	37.04	1.45
3	0.30	430	996	37.41	11.22	14.96	34.88	1.5
4	0.40	430	1024	35.24	10.57	14.10	38.68	1.4

4 CONCLUSIONS

The following conclusions is obtained:

1. The increase in vortex strength can be correlates with increase in temperature of combustion zone as equivalence ratio increases.
2. The higher temperature near to throat section is observed due to higher concentration of oxygen leading to combustion. Finally slightly lower temperature as compared to throat section is seen in reduction zone of gasifier. This is because of hot gases are reduced by unreacted char in this zone.
3. The results leads to conclusion that there is an optimal value of equivalence ratio about 0.3 producing best quality of syngas.

REFERENCES

- A. Silaen, T.Wang. , 2010 , Effect of Turbulence and Devolatilization Model on Coal Gasification Simulation in an Entrained Flow Gasifier, *International Journal of Heat and Mass Transfer*, 53(2074-2091).
- C. Chen, M. Horio, T. Kojima. , 1999 , Numerical Simulation of Entrained Flow Coal Gasifier part-1 Modeling of Coal Gasification in an Entrained Flow Gasifier, *Chemical Engineering Science*, 35(3861-3874).
- T. Reed, A. Das. , 1988 , Handbook of Downdraft Gasifier Engine System, 1st edition, *Biomass Energy Foundation Press*.
- V. Patel, D. Upadhya, R. Patel. , 2014 , Gasification of Lignite in a Fixed bed Reactor: Influence of Particle Size on Performance of Downdraft Gasifier, *Energy*, 78(323-332).

Design and analysis of heat pipe heat exchanger for stenter machine

H V Mardhekar

Proterm Assistant Professor, Mechanical Engineering Department, Marwadi Education Foundation Group of Institutions

S.V. Jain

Associate Professor, Mechanical Engineering Department, Institute of Technology Nirma University

V.J.Lakhera

Professor, Mechanical Engineering Department, Institute of Technology Nirma University

Dr.R.N.Patel

HOD and Professor, Mechanical Engineering Department, Institute of Technology Nirma University

ABSTRACT: Stenter machine uses air to air heat exchanger as heat recovery unit from the high-temperature exhaust gases. In the present study, the design of heat pipe heat exchanger is presented for the Stenter machine. The materials of the heat pipe, wick and fin were proposed as Copper, Stainless Steel and Aluminum respectively. Depending on requirements, 4 different options of heat pipe heat exchangers are proposed. To predict the performance of the heat pipe heat exchanger, the heat pipe is fabricated and experiments were performed at different flow rates and inclinations of the heat pipe. The analysis was done by recirculating the water through the heat exchanger, passing the water once through heat exchanger as well as with stagnant water. The collection efficiency and instantaneous efficiency of heat pipe were obtained in the range of 47-49% and 85-94% respectively for different flow rates.

1 INTRODUCTION

Stenter machine is used for stretching of fabrics to bring the length and width to predefined dimensions. It is also used for heat setting of fabric and for applying chemicals for shade variation. Heat exchangers are used for waste heat recovery in the Stenter machine. The heat pipe is an element for heat transfer in which wick and working fluid are provided under vacuum. Heat pipes can have several hundred times more thermal conductivity than the pipe of the same material and hence it is also sometimes referred as a superconductor.

Srimuang and Amatachaya (2012) reviewed the applications of heat pipe heat exchangers for the heat recovery in air preheater for energy saving in industrial applications. Some other applications of heat pipe heat exchanger are also shown. Borges et al. (2011) described the use of heat pipe heat exchanger for Stenter machine's exhaust maintained at 100-200°C. Heat pipe heat exchanger was designed for the heat recovery from the exhaust gases. For calculation of heat and mass balance in Stenter machine and hot-air generator, a routine was developed and implemented in EES. For designing of heat pipe, TROCATER software was used. Shah and Giovannelli (1988) described characteristics of different types of heat pipes. For complete design procedure of heat pipe heat exchanger NTU method was explained. The details of material selection, working fluid, types of wick etc. are also discussed.

In this paper, the design and optimization of heat pipe heat exchanger are presented. The optimized HPHE was fabricated and parametric studies were done by varying flow rates, power inputs and inclinations of the heat pipe.

2 DESIGN OF HEAT PIPE HEAT EXCHANGER

2.1 Major specifications and design methodology

The major design specifications and constraints in the design are given in Table 1.

Table 1. Design specifications for heat pipe heat exchanger.

Parameter	Description
Heat transfer medium	Air to air
Temperature range in exhaust gas	80°C (min) to 200°C (max)
Flow rate of exhaust air	3000 m ³ /hr (Design)
Flow rate of fresh air	1000 m ³ /hr (min)
Weight of Heat transfer unit	upto 450 kg
Pressure drop across HRU	1 mm H ₂ O (max)
Imported parts	Less imported parts.
Corrosion effect	Use of corrosion resistant material.
Oil condensation	Provision for managing condensed oil.

Designing of heat pipe heat exchanger involves designing and analysis of air side of heat exchanger followed by the designing of the heat pipe. The steps to design heat pipe heat exchanger are given below (Shah & Giovannelli, 1988):

- To find out the effectiveness and NTU of the heat exchanger.
- To fix the pipe dimensions and pitch of heat exchanger.
- To decide the pressure drop and to find out the mass velocity of air and hot gases entering the heat exchanger.
- To find Reynolds number of the heat exchanger.
- To find heat transfer coefficient and overall heat transfer coefficient of the heat exchanger.
- To find out dimensions of heat exchanger and number of heat pipes required for heat transfer.
- To find out actual pressure drop and iterating until decided pressure drop is achieved by varying the Reynolds number of the heat exchanger.
- To design the heat pipe.

3 GOVERNING EQUATIONS

3.1 Design of heat pipe heat exchanger (Shah & Giovannelli, 1988)

The number of transfer units (NTU) was found out using

$$NTU = \frac{1}{1-C^*} * \ln \left[\frac{1-C^* \epsilon}{1-\epsilon} \right] \quad (1)$$

where, C* = Heat capacity ratio, C = Heat capacity (kJ/kg.K), ϵ = Effectiveness.

The mass velocity was found out using

$$G = \left[\frac{2g_c \Delta p}{Deno} \right]^{1/2} \quad (2)$$

$$Deno = \frac{f}{J} ntu pr^{2/3} \left(\frac{1}{\rho m} \right) + 2 \left[\frac{1}{\rho o} - \frac{1}{\rho i} \right] \quad (3)$$

where, G = Mass velocity (kg/m².s), g_c = Proportionality constant, ρ = Density (kg/m³), f = Friction factor, J = Colburn factor, Pr = Prandtl number.

Reynolds number was found out using

$$Re = \frac{G Dh}{\mu} \quad (4)$$

where Dh = Hydraulic diameter (m), μ = Viscosity (kg/ms).

Heat transfer coefficient was found out by

$$h = \frac{J G C_p}{Pr^{2/3}} \quad (5)$$

Overall heat transfer coefficient was found out by

$$\frac{1}{U} = RA = \frac{1}{\eta_o h} + \frac{R_s}{\eta_o} + \frac{r_o - r_i}{k_p} \frac{A}{A_{bp}} + \frac{r_i - r_v}{k_e} \frac{A}{A_{ws}} \quad (6)$$

where, A = Area (m²), η = Efficiency, R_s = Scaling resistance, K = Conductivity (W/m°C).
Number of heat pipes were found out using

$$q_{HP} = q_{HX}/N_t \quad (7)$$

Minimum free flow area of one side of fluid is given by

$$A_o = (m/G) \quad (8)$$

where, m = Mass flow rate (kg/s), A_o = Minimum free flow area of one fluid (m²).

Frontal area of heat exchanger is given by

$$A_{fr} = A_o/2 \quad (9)$$

where, A_{fr} = Frontal flow area of the heat exchanger (m²).

Geometrical dimension L₂ is given by

$$L_2 = \frac{D_h A}{4A_o} \quad (10)$$

where, A = Total area of heat transfer required (m²).

Geometrical dimension L₃ is given by

$$L_3 = \frac{A_{fr,e}}{L_{1,e}} \quad (11)$$

Minimum thickness of heat pipe is given by

$$\delta_{min} = \Delta P d_o / 2 S_u \quad (12)$$

where, d_o = Outer diameter of the heat pipe, S_u = Ultimate strength of heat pipe material.

3.2 Design of heat pipe (Reay & Kew. 2006)

For correct working of heat pipe the following condition should be satisfied

$$\Delta P_c \geq \Delta P_l + \Delta P_v + \Delta P_g \quad (13)$$

where, Maximum capillary pressure $\Delta P_c = \frac{2\sigma_l \cos \theta}{r_e}$ (14)

Pressure drop of liquid in the wick $\Delta P_l = \frac{\mu_l Q l_{eff}}{\rho_l L A_w K}$ (15)

Pressure drop due to gravitation $\Delta P_g = \rho g l \sin \phi$ (16)

Pressure drop required for vapor flow $\Delta P_v = \frac{8 \mu_v m l_{eff}}{\rho \pi r_v^4}$ (17)

Sonic limit check for heat pipe is given by

$$Q_s = A_v L \rho_v \left[\frac{1 + \gamma_v}{2 + \gamma_v} \right] (\gamma_v R T_v)^{0.5} \quad (18)$$

Boiling limit check for heat pipe is given by

$$Q_b = 2\pi * l_e * K_e * T_v * Nt \left[2 * \frac{\sigma_l}{r_n} - p_c \right] L * \rho_v \ln(r_i/r_v) \quad (19)$$

Entrainment limit check for heat pipe is given by

$$Q_{ent} = \pi r_v^2 L \sqrt{\frac{2 \pi \rho_v \sigma_l}{z}} \quad (20)$$

where, L = Latent heat of vaporization (kJ/kg), σ = Surface tension on liquid surface (N/m), z = Characteristic number, Q = Power (kW), φ = Inclination of heat pipe, r_v = Vapor core radius(m).

Based on above equations, four different heat pipe heat exchangers were designed. The materials of the heat pipe, wick and fin were taken as Copper, Stainless-steel and Aluminum respectively. The major dimensions of these options are given in Table 2 and the three-dimensional models of these options are shown in Fig. 1 (Mardhekar, 2015).

Table 2. Options of heat pipe heat exchangers.

Parameters	Option 1	Option 2	Option 3	Option 4
Fins / Inch	Hot side : 8.8 Cold side : 8.8	Hot side : 4 Cold side : 4	Hot side : 4 Cold side : 4	Hot side : 0 Cold side : 8.8
No. of heat pipes	60	135	112	210
Outer dia. of heat pipe	0.0254 m	0.0254 m	0.0254 m	0.0254 m
Diameter of Fin	0.04411 m	0.04411 m	0.04411 m	0.04411 m
Thickness of Fin	3.04×10^{-4} m	3.04×10^{-4} m	3.04×10^{-4} m	3.04×10^{-4} m
Reynolds No	Hot Side : 272 Cold Side : 400	Hot Side : 570.6 Cold Side : 839	Hot Side : 987.6 Cold Side : 1507	Hot Side : 2731 Cold Side : 400
Overall heat transfer coefficient	9.749 W/m ² K	8.819 W/m ² K	10.907 W/m ² K	2.85 W/m ² K
Pressure drop	3.323 Pa	3.274 Pa	16.93 Pa	0.4353 Pa
Width L ₁	1.2095 m	1.2095 m	1.2095 m	1.2095 m
Depth L ₂	0.1025 m	0.2377 m	0.3367 m	0.3429 m
Height L ₃	1.4663 m	1.33 m	0.7542 m	1.5 m

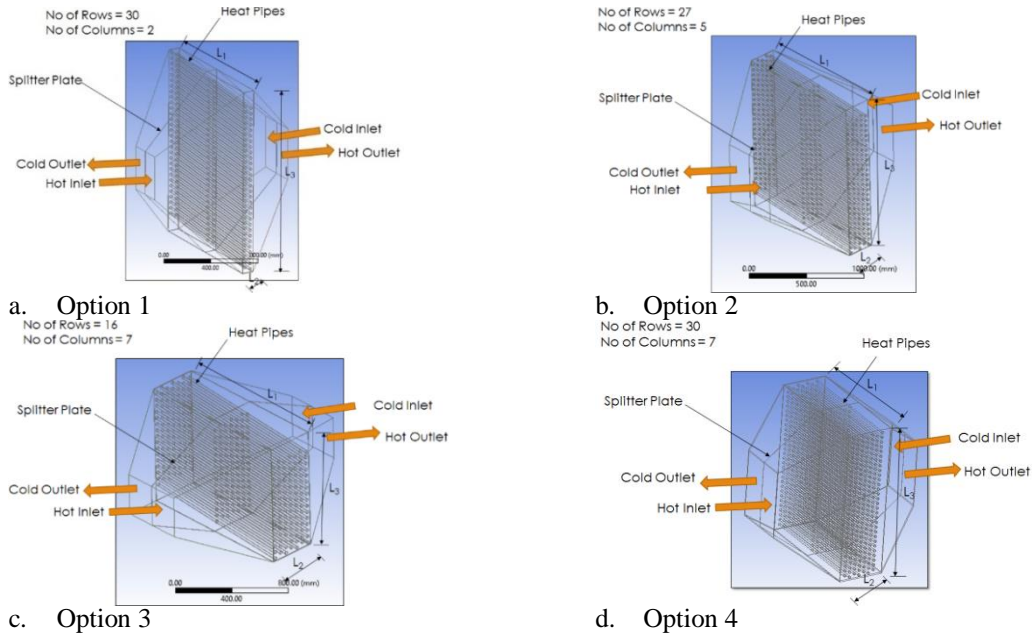


Figure 1. Models for different options of heat pipe heat exchanger.

4 EXPERIMENTAL INVESTIGATIONS ON HEAT PIPE

After the design optimization, 2 numbers of heat pipes (outer dia. 0.0254 m, 4 fins/inch) were fabricated. The parametric studies on heat pipe were carried out as under:

- by recirculating the water in closed loop test rig
- by passing the water once through the shell
- with stagnant water at different power inputs and inclinations of the heat pipe

The schematic diagram and experimental setup are shown in the Fig. 2.

The collection efficiency of heat pipe was worked out using Eq. (21).

$$\eta = \frac{\text{Heat gained by water}}{\text{Electric heat supplied}} = \frac{m c_p \Delta T}{V I \cos \phi} \quad (21)$$

where, m = mass flow rate of water (kg/s), C_p = specific heat of water (J/kgK), ΔT = rise in water temperature, V = voltage (V), I = current (A), $\cos\phi$ = power factor.

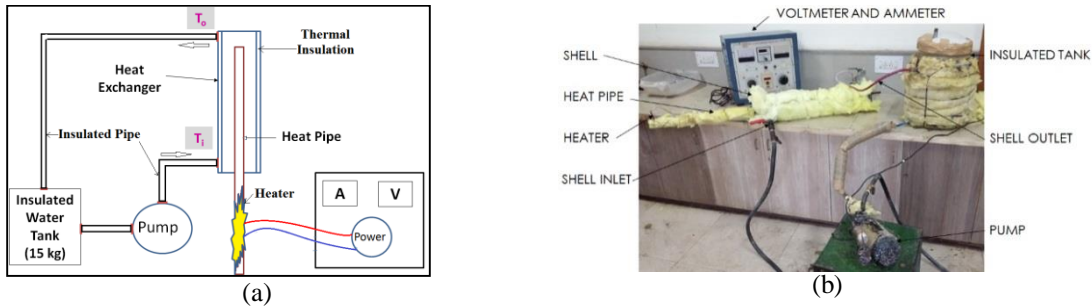


Figure 2. (a) Schematic diagram and (b) experimental setup.

From the experiments, the time required to reach to steady state for heat pipe was found as 135 minutes. The instantaneous efficiency of heat pipe was found in the range of 85-94% at different flow rates (0.0070 - 0.016 kg/s). The efficiency of the heat pipe at different inclinations ($90^\circ, 70^\circ, 4.5^\circ$) and power input (155 – 425 W) was found in the range of 87-97%. The variation of water temperature against time is shown in Fig. 3(a) and variation of efficiency with different heat inputs is shown in Fig. 3(b) (Mardhekar, 2015).

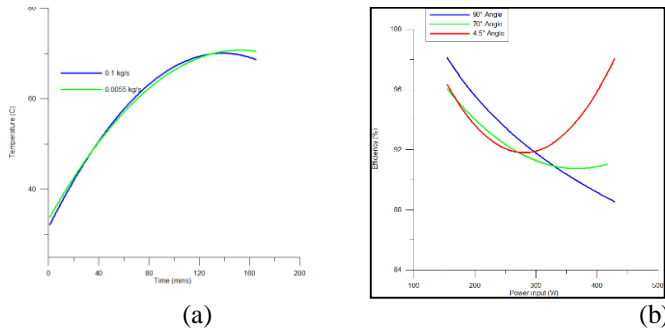


Figure 3. Variation of (a) temperature versus time (b) efficiency versus power input.

5 CONCLUSIONS

Based on the design, Copper heat pipes with 1 layer of Stainless Steel wick and Aluminum fins are recommended. It was concluded that the Option 2 (135 heat pipes with 4 fins/inch on hot and cold sides) can be used in the applications where low fluff and lint are expected in the exhaust gases going inside the heat exchanger. However, for the Stenter machine subjected to high fluff and lint Option 4 (210 heat pipes with 8.8 fins/inch on cold side and bare hot side) can be used to avoid clogging on hot side. The instantaneous and collection efficiency of heat pipe was found in the range of 85-94% and 47-49% and at different flow rates and time required to reach steady state is 135 minutes.

REFERENCES

- Borges, T., Pickler, G. & Henriques, M. , 2011, Heat pipe air heaters in stenters for textile industry, *21st Brazilian congress of mechanical engineering*: 24-28.
- Mardhekar, H.V. , 2015, Design and analysis of heat pipe heat exchanger for stenter machine, M Tech Thesis, Nirma University.
- Reay, D. & Kew, P. , 2006, *Heat pipes theory design and applications*. Burlington: USA.
- Shah, R. & Giovannelli, A. 1988. Heat pipe heat exchanger design theory, Heat transfer equipment design: 609-653.
- Srimuang, W. & Amatachaya. P. , 2012 , A review of the applications of heat pipe heat exchangers for heat recovery, *Renewable and Sustainable Energy Reviews* 16: 4303-4315.

Identification of Energy Saving Potential of Different Thermal Insulation through Mathematical Modelling

Somakshi Mattoo,

M.Tech Student, Institute of Technology, Nirma University, Ahmedabad, Gujarat, India

B A Shah

Assistant Professor, Institute of Technology, Nirma University, Ahmedabad, Gujarat, India

A M Lakdawala

Associate Professor, Institute of Technology, Nirma University, Ahmedabad, Gujarat, India

ABSTRACT: In the present work, a mathematical model is developed to demonstrate energy saving potential of a thermally insulated, air conditioned room and identify the best insulation. Solar radiation and cooling capacity of air conditioner are applied as boundary conditions of the room. The room is discretised using Finite Volume Method and governing equations are solved simultaneously. A code is developed to calculate the mean temperature inside the room and AC working time. Simulations have been carried out for four different conductivities and seven different thicknesses of insulations namely Polyurethane Foam, Extruded Polystyrene Foam, Fiberglass and Rockwool. AC on-off cycle for different insulations and thicknesses, 2-D temperature contour variations and velocity profiles are generated as outcome of the code. The amount of energy saved is calculated on the basis of how long the AC works. A graph is plotted for Cost of electrical energy saved per day vs thickness of insulated wall for different insulation and optimum thickness of insulated wall is obtained from it.

Keywords: Energy Saving Potential, Conjugate heat transfer, AC On-Off Cycle, Cost of Electrical Energy Saved/Day, Optimum Thickness of Insulation

Nomenclature

X Non-dimensional horizontal coordinate
 Y Non-dimensional vertical coordinate
 Z Non-dimensional transverse coordinate
 U Non-dimensional velocity of fluid in x -direction
 V Non-dimensional velocity of fluid in y -direction
 W Non-dimensional velocity of fluid in z -direction
 \mathbf{U} Non-dimensional velocity vector
 P Non-dimensional pressure
 g Acceleration due to gravity
 T_s Hot wall temperature
 T_∞ Free stream temperature inside room

L Characteristic length of enclosure
 Pr Prandtl number
 Gr Grashof number
 Ra Rayleigh number

Greek symbols

θ Non-dimensional temperature
 ρ Density of fluid (air)
 τ Non-dimensional time
 α Thermal diffusivity
 β Thermal expansion coefficient
 ν Kinematic viscosity

1 INTRODUCTION

The world's energy resources are fast depleting with the rapidly increasing consumption of the growing population, thus creating a need to develop methods for saving or optimization of these resources. Use of thermal insulation is an efficient way of conserving energy to bridge the gap between energy demand and supply. Insulation material is important tool for constructing energy conserving buildings. The better the insulation, the better resistance it will provide to the heat transfer in and out of the insulated room.

In an air conditioned room heat gain through walls, roofs, ceilings etc. are major source of heat gain including heat gain through glass and others. The conduction heat transfer through wall or roof depend on wall thickness and thermal conductivity of material used. Thus there is a large scope of energy saving is possible by providing thermal insulation on wall and roof of an air conditioned room. Conjugate heat transfer is fundamental for many devices and processes, including heat exchange between building and environment, heat exchangers, material processing and many others (Zhao 2006). A large number of studies have been reported on conjugate heat transfer in square, triangular, rectangular or open cavities with different fluids and thermal boundary conditions, square and open cavities being more common (Ha 2000, Serrano-Arellano 2014). This study aims to develop code to find AC on/off cycle in a close insulated room and thereby calculate energy saving potential of different thermal insulation of varying thickness.

2 MATHEMATICAL MODELLING

In the present work a cubic room with dimensions 3m x 3m x 3m without any doors or windows, which is maintains temperature at 25° C using an air conditioner, have been considered. The inside of the room is thermally insulated on all sides. Aim of the project is to identify energy saving potential of different thermal insulation by mathematical modelling. Different thermal insulation have different value of thermal conductivity, k. The inside wall temperature of the room is determined by solar radiation falling on the walls and roof of the room which varies with time and place. A code is prepared to calculate the mean temperature of the different points (nodes) inside the room using governing equations. When the temperature reaches a temperature of 25° C, the AC gets cut-off and switches on when the temperature reaches 27°C. Figure 1 shows a three-dimensional view of the insulated room described in the problem.

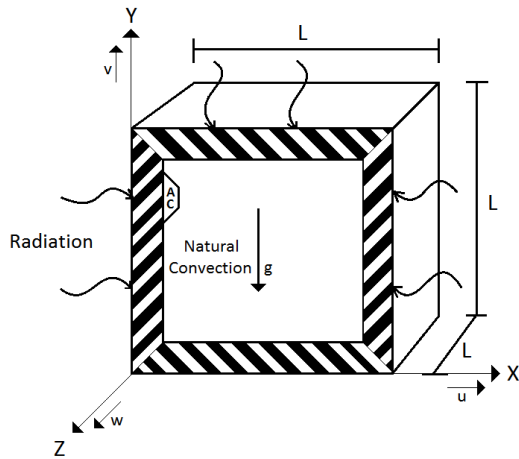


Figure 1. 3D view of insulated room

2.1 Governing Equations in Non-Dimensional Form

In the present work non-dimensional form of governing equations are solved. Governing equations are non-dimensionalised (normalised) by using scaling constants for length as L , for velocity as a/L , for pressure as $\rho\alpha^2 / L^2$ temperature as $(T_s - T_\infty)$ and time as L^2 / α .

$$X = \frac{x}{L}, Y = \frac{y}{L}, Z = \frac{z}{L}, U = \frac{uL}{\alpha}, V = \frac{vL}{\alpha}, W = \frac{wL}{\alpha}, P = \frac{pL^2}{\rho\alpha^2}, \theta = \frac{T - T_\infty}{T_s - T_\infty}, \tau = \frac{t\alpha}{L^2}$$

Continuity equation in non-dimensional form for an incompressible fluid can be written as

$$\frac{\partial U}{\partial X} + \frac{\partial V}{\partial Y} + \frac{\partial W}{\partial Z} = 0 \quad (1)$$

Momentum equation in non dimensional form for an incompressible unsteady fluid can be written as

$$\frac{\partial \mathbf{U}}{\partial \tau} + U \frac{\partial \mathbf{U}}{\partial X} + V \frac{\partial \mathbf{U}}{\partial Y} + W \frac{\partial \mathbf{U}}{\partial Z} = Pr \left(\frac{\partial^2 \mathbf{U}}{\partial X^2} + \frac{\partial^2 \mathbf{U}}{\partial Y^2} + \frac{\partial^2 \mathbf{U}}{\partial Z^2} \right) - \frac{\partial P}{\partial X} \hat{i} - \frac{\partial P}{\partial Y} \hat{j} - \frac{\partial P}{\partial Z} \hat{k} + Ra Pr \theta \hat{j} \quad (2)$$

$$\text{where } Pr = \frac{\nu}{\alpha}, \quad Gr = \frac{g\beta(T_s - T_\infty)L^3}{\nu^2}, \quad Ra = Gr \cdot Pr = \frac{g\beta(T_s - T_\infty)L^3}{\nu\alpha}$$

Pr , Gr and Ra are the governing non-dimensional parameters. Boussinesq approximation is used in the Navier-Stokes (momentum) equation in the pressure gradient term. Variation in density due to temperature variation generates the buoyancy force causing flow of air inside the room resulting in heat transfer by natural convection.

Energy Equation in non dimensional form for an incompressible unsteady fluid can be written as

$$\frac{\partial \theta}{\partial \tau} + U \frac{\partial \theta}{\partial X} + V \frac{\partial \theta}{\partial Y} + W \frac{\partial \theta}{\partial Z} = \left(\frac{\partial^2 \theta}{\partial X^2} + \frac{\partial^2 \theta}{\partial Y^2} + \frac{\partial^2 \theta}{\partial Z^2} \right) \quad (3)$$

Three boundary conditions are applied on the problem at hand to calculate the temperature at different points (nodes) inside the thermally insulated room. First is the **solar radiation** falling on the walls and roof of the room, which is used to calculate inside wall temperature. Second is the **no-slip condition** at the walls. Velocity of the fluid at the walls (boundary) of the room is zero, i.e. $U=0$, $V=0$, $W=0$. But there is movement of fluid (air) in the y -direction (v -velocity) inside the room arising due to buoyancy force (due to temperature variation) which is taken into account in the Y -Momentum (Navier-Stokes) Equation. The third is the **constant wall heat flux** dissipated by the AC.

2.2 Numerical Methodology

The governing equations are discretised using finite volume method on a staggered grid where the pressure is located at the cell center whereas the velocity components u and v are staggered and located at the cell face centers. The finite volume discretised form of navier-stokes equation is

$$\frac{\Delta V (\mathbf{U}^{n+1} - \mathbf{U}^n)}{\Delta \tau} = F^D - F^C - \nabla P^{n+1} \Delta S + F_g \quad (4)$$

where **Convective Flux** $F^C = \nabla \mathbf{U} (\mathbf{U} \cdot \Delta S)$, **Diffusive Flux** $F^D = Pr \nabla (\nabla \mathbf{U} \cdot \Delta S)$ and **Gravitational Force** $F_g = \Delta V (Ra \cdot Pr \cdot \theta) \hat{j}$

In the present work, \mathbf{U} in the convective flux is calculated using the total variation diminishing (TVD) scheme. The gradient of velocity across a cell face in diffusion flux term is calculated using central difference scheme.

The projection method is used to solve time-dependent Navier-Stokes equation for incompressible fluids. The main advantage of this technique is that the pressure and velocity field computations are decoupled.

Navier-Stokes equation (dimensionless form) for an incompressible fluid can be written as:

$$\frac{\partial \mathbf{U}}{\partial \tau} + (\mathbf{U} \cdot \nabla) \mathbf{U} = -\nabla P + Pr \nabla^2 \mathbf{U} + Ra Pr \theta \hat{j} \quad (5)$$

where vector velocity, $\mathbf{U} = U\hat{i} + V\hat{j} + W\hat{k}$ and the term $RaPr\theta_j = 0$ for Navier-Stokes equation in x- and z-direction (U and W velocities respectively).

$$\frac{\mathbf{U}^{n+1} - \mathbf{U}^n}{\Delta\tau} = -(\mathbf{U}^n \cdot \nabla)\mathbf{U}^n - \nabla P^{n+1} + Pr\nabla^2\mathbf{U}^n \quad (6)$$

Computation of the intermediate velocity, \mathbf{U}^* , is done explicitly by ignoring the pressure gradient term in the momentum equation.

Velocities at new time level, n+1 can be calculated by substituting the Pressure of new time level. Thus, the system has updated values for the new time level. Values of U , V , W and P at different nodes inside the room can be calculated by this method. These values can be substituted in the Non-dimensional Energy Equation and value of θ can be computed which further gives the value of temperature T at different nodes.

3 RESULTS AND DISCUSSION

In the present study only solar radiation data for a day (per day) in summer in Ahmedabad is considered and all the results obtained below are for Ahmedabad only. 2 D heat transfer is considered in the room. Thickness of bare (uninsulated) walls & roof is considered to be 0.1 m, to which the insulation thickness is added. Conductivity k and thickness of wall with insulation Δx is varied. *Polyurethane Foam (PUF)*, *Extruded Polystyrene Foam (XPS)*, *Fiberglass and Rockwool insulations* having conductivities 0.021 W/mK, 0.033 W/mK, 0.04 W/mK and 0.045 W/mK respectively are used by varying thickness as 0.125, 0.15, 0.175, 0.2, 0.225, 0.25 & 0.275 m for each insulation.

3.1 Variation of AC On-Off Cycle with Insulation

In the present work, it is considered that an AC of cooling capacity 1 ton is installed on the west wall of the insulated room. Accordingly the west side wall acts as a sink for the hot air inside the room and dissipates it to the surroundings. The AC switches on when the mean temperature in the room reaches 27°C and the AC switches off when the mean temperature in the room reaches 25°C. AC on-off cycle (time step) is generated by the code showing the duration for which the AC is on (working) and the time for which it is off. In the cycle 0 and 1 represent the off and on condition (time) of the AC respectively.

The AC working (on) time increases with the increase in conductivity of insulation material and decreases with the increase in thickness of the material. The mean temperature inside the room rises quickly as a result of increase in conductivity and decrease in thickness of the insulation material and attains the AC switch on temperature. Thus, the AC works for a longer time to achieve the required (switch off) temperature.

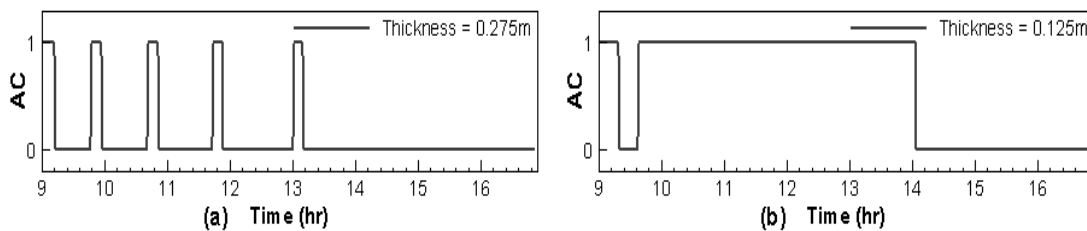


Figure 2. AC On-Off Cycles for (a) Polyurethane Foam (PUF) insulation at insulated wall thickness of 0.275m and (b) Rockwool insulation at insulated wall thickness of 0.125m

3.2 Calculation of Optimum Thickness of Insulation

The AC installed at the wall in the insulated room under study is of capacity 1 ton (3.517 kW) and 3-star rating. Compressor work (power input) of the AC is calculated by dividing the refrigeration capacity (output) of the AC with Energy Efficiency Ratio (EER) which comes out to be

0.983 kW (Data of Carrier 3-star AC is used). Energy is consumed in the form of electricity. Cost of electricity (energy) for Ahmedabad is taken as Rs 3.2 per unit (kWh). Data from the AC on-off cycles is used for calculating the values in the graphs in Figure 5 which are used to determine the optimum thickness for each insulation.

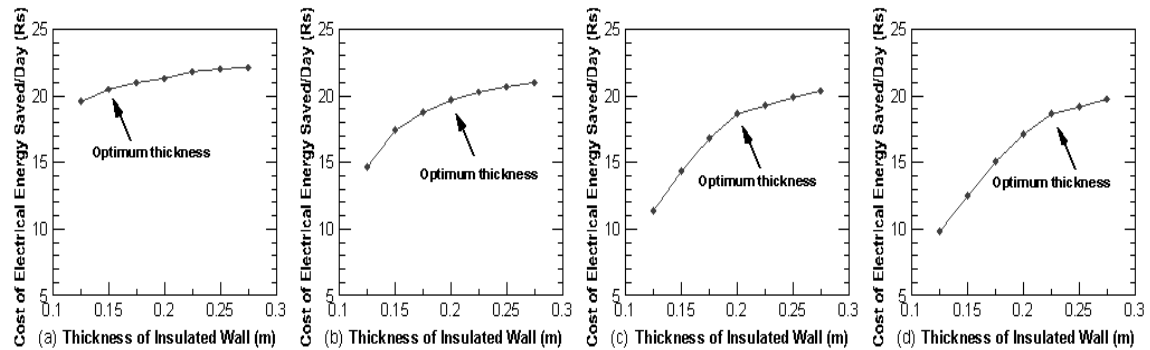


Figure 3. Cost vs Thickness Variation for (a) Polyurethane Foam, (b) Extruded Polystyrene Foam, (c) Fiberglass and (d) Rockwool

4 CONCLUSION

- A graph is plotted for Cost of electrical energy saved/day (Rs) vs Thickness of insulated wall (m) for different insulations and optimum thickness of insulated wall is obtained from it. Energy saved is directly proportional to the thickness of insulation used and inversely proportional to the conductivity of insulation. This means the AC working time and energy consumption can be reduced by decreasing the conductivity of the insulated wall or increasing the thickness of the insulation.
- Optimum thicknesses for Polyurethane Foam (PUF), Extruded Polystyrene Foam (XPS), Fiberglass and Rockwool insulation are found to be 0.15 m, 0.2 m, 0.2 m and 0.225 m respectively.
- Saving in cost of electricity is found to be maximum for Polyurethane Foam insulation with conductivity, $k = 0.021 \text{ W/mK}$ at insulated wall thickness of 0.275 m and minimum for Rockwool insulation with conductivity, $k = 0.045 \text{ W/mK}$ at insulated wall thickness of 0.125 m.

REFERENCES

- Ha, M.Y. & Jung, M.J. , 2000 , A numerical study on three-dimensional conjugate heat transfer of natural convection and conduction in a differentially heated cubic enclosure with a heat-generating cubic conducting body. *Int. J of Heat & Mass Transfer* 43: 4229-4248.
- Incropera, F.P. & DeWitt, D.P. (5th ed.), 2002 , *Fundamentals of Heat and Mass Transfer*. New York: Wiley.
- Papadopoulos, A.M. , 2005 , State of the art in thermal insulation materials and aims for future developments. *Energy and Buildings* 37: 77–86.
- Serrano-Arellano, J. & Gijón-Rivera, M. , 2014 , Conjugate heat and mass transfer by natural convection in a square cavity filled with a mixture of Air–CO₂. *Int. J. of Heat & Mass Transfer* 70: 103–113.
- Sukhatme, S.P. & Nayak, J.K. (3rd ed.) , 2008 , *Solar Energy Principles of Thermal Collection and Storage*. Tata McGraw-Hill Companies.
- Versteeg, H. & Malalasekera, W. (2nd ed.) , 2007 *An Introduction to Computational Fluid Dynamics: The Finite Volume Method*. Pearson.
- Zhao, F.Y., Tang, G.F. & Liu, Di. , 2006 , Conjugate natural convection in enclosures with external and internal heat sources. *Int. J. of Engineering Science* 44: 148–165.